Author Manuscript

Author Manuscript

Author Manuscript

Author Manuscript

HHS Public Access

Author manuscript

*J Immunol*. Author manuscript; available in PMC 2023 April 01.

Published in final edited form as:

*J Immunol*. 2022 April 01; 208(7): 1566–1584. doi:10.4049/jimmunol.2101056.

# Preclinical analysis of candidate anti-human CD79 therapeutic antibodies using a humanized CD79 mouse model

**Scott M. Wemlinger**[*], **Chelsea R. Parker Harp**[†], **Bo Yu**[‡], **Ian R. Hardy**[§], **Matthew Seefeldt**[¶], **Jennifer Matsuda**[‖], **Michael Mingueneau**[†], **Kerri A. Spilker**[#], **Thomas O. Cameron**[#], **James W. Larrick**[‡], **Andrew Getahun**[*], **John C. Cambier**[*]

[*]Department of Immunology and Microbiology, University of Colorado Denver, Anschutz Medical Campus, Aurora, CO, USA

[†]Multiple Sclerosis and Neurorepair Research Unit, Biogen, Cambridge, MA, USA

[‡]Panorama Research Institute, Sunnyvale, CA, USA

[§]Miltenyi Biotech, Bergisch Gladbach, Germany

[¶]The Charles Gates Biomanufacturing Facility, Aurora, CO, USA

[‖]Department of Biomedical Research, National Jewish Health, Denver, CO, USA

[#]Biologics Drug Discovery, Biogen, Cambridge, MA, USA

## Abstract

The B cell antigen receptor (BCR) comprises a membrane bound immunoglobulin that is non-covalently associated with a heterodimer of CD79A and CD79B. While the BCR immunoglobulin component functions to sense extracellular antigen, CD79 subunits contain cytoplasmic immunoreceptor tyrosine-based activation motifs (ITAMs) that mediate intracellular propagation of BCR signals critical for B cell development, survival, and antigen-induced activation. CD79 is therefore an attractive target for antibody and CAR-T therapies for autoimmunity and B cell neoplasia. While the mouse is an attractive model for preclinical testing, due to its well-defined immune system, an obstacle is the lack of cross-reactivity of candidate therapeutic anti-human monoclonal antibodies with mouse CD79. To overcome this problem we generated knock-in mice in which the extracellular, immunoglobulin (Ig)-like domains of CD79A and B were replaced with human equivalents. Here we describe the generation and characterization of mice expressing chimeric CD79 and report studies that demonstrate their utility in preclinical analysis of anti-human CD79 therapy. We demonstrate: human and mouse CD79 extracellular domains are functionally interchangeable; anti-human CD79 lacking Fc region effector function does not cause significant B cell depletion, but induces 1) decreased expression of plasma membrane-associated (m)IgM and mIgD, 2) uncoupling of BCR-induced tyrosine phosphorylation and calcium mobilization, and 3) increased expression of PTEN, consistent with the levels observed in anergic B cells. Finally, anti-human CD79 treatment prevents disease development in two mouse models of autoimmunity. We also present evidence that anti-human CD79 treatment may inhibit antibody secretion by terminally differentiated plasmablasts and plasma cells, *in vitro*.

Corresponding author John C. Cambier, John.Cambier@cuanschutz.edu, 303-724-8663.

Author Manuscript Author Manuscript Author Manuscript Author Manuscript

**Keywords**

Anti-human CD79; CD79-targeted therapy; B cells; Anergy; Autoimmunity; Experimental Autoimmune Encephalomyelitis; Systemic Lupus Erythematosus

## Introduction

Cell surface expression of pre- and mature B cell antigen receptors (BCRs), as well as development and maturation of B cells in the bone marrow, is dependent on expression of CD79 [1]. Similarly, productive signaling of these outcomes by the BCR requires the presence of ITAMs contained within the cytoplasmic domains of CD79A and CD79B [2] [3]. Membrane-bound immunoglobulin molecules, e.g. IgM, IgD, and IgG, pair with heterodimers of CD79A/B via non-covalent transmembrane domain interactions [4] (Fig 1A). Aggregation of BCR by multimeric antigens initiates phosphorylation of CD79 ITAM tyrosine's leading to recruitment and activation of proximal tyrosine kinases Lyn and Syk that nucleate downstream signaling and ultimately drives B cell activation [5].

CD79 expression is restricted to B lineage cells. CD79A (*mb-1*, Ig-alpha, $Ig_{\alpha}$) and CD79B (*B29*, Ig-beta, $Ig_{\beta}$) are single-spanning, transmembrane proteins covalently associated by a disulfide bond [6] [7]. Greatest conservation of amino acid sequences between human and mouse CD79 is found in the transmembrane and cytoplasmic domains, 89%, A; 96%, B (Fig 1B). Reduced homology in the extracellular domains (57%, A; 55%, B) facilitates mouse immune responsiveness to non-cross reactive human CD79 epitopes. Such murine antibodies can be humanized for therapeutic application.

The potential utility of anti-CD79 antibodies for therapeutic intervention has been demonstrated in mouse models of autoimmunity including collagen-induced arthritis and MRL/*lpr* lupus [8] [9] [10]. In 2014, Hardy et. al. described a form of polyclonal B cell anergy that can be induced using anti-mouse CD79 monoclonal antibody and could be exploited for therapeutic purposes [9]. Selected anti-CD79 antibodies act as "reverse agonists", inducing BCR desensitization. Importantly, mutant mouse IgG2a antibody lacking the ability to mediate antibody-dependent cell-mediated cytotoxicity (ADCC) and complement-dependent cytotoxicity (CDC) was shown to prevent collagen-induced arthritis, while not inducing B cell depletion. This polyclonal anergy is lost upon decay of the antibody *in vivo*. Thus, the mechanism of action of ADCC- and CDC-incompetent anti-CD79 is distinct from anti-CD20, which acts by depleting B cells. The utility of B cell depleting therapy in humans has been demonstrated using several iterations of CD20 directed therapies in indications including but not limited to multiple sclerosis [11] [12], type 1 diabetes [13], rheumatoid arthritis [14], lupus [15], and neuromyelitis optica [16] [17]. The success of anergizing CD79-targeted therapies is predicted by these examples. Because they are non-depleting and reversable, anti-CD79 therapies should have improved safety relative to anti-CD20 [18]. A murine model in which to conduct preclinical testing of candidate anergizing anti-human CD79 antibodies would be an invaluable tool for defining their mechanism of action and potential clinical utility.

Author Manuscript Author Manuscript Author Manuscript Author Manuscript

Here we describe the generation and characterization of human CD79 extracellular domain knock-in mice and validation of their use in studying anti-CD79 therapies for potential application in human autoimmune disease. B cell development and function is normal in these mice and a desensitizing anti-human CD79 antibody treatment blocks pristane-induced production of anti-chromatin autoantibodies. Additionally, prophylactic treatment in the experimental autoimmune encephalomyelitis (EAE) model with non-B cell depleting anti-human CD79 antibody significantly reduced disease severity and led to complete recovery.

## Materials and methods

### Human and animal use

All experiments involving mice were performed in accordance with the regulations and with approval of the University of Colorado Denver Institutional Animal Care and Use Committee. Samples from human subjects were obtained with informed consent prior to inclusion in the study at the University of Colorado Anschutz Medical Center using protocols approved by the University of Colorado Institutional Review Board.

### Chimeric CD79A targeting construct design

Constructs were assembled using BAC recombineering techniques including Red recombination and cleavage with homing endonuclease I-SceI. In order to generate mice expressing human-mouse chimeric CD79A (cCD79A), targeting constructs were designed in which amino acids (aa) 29–160 of mouse CD79A were replaced by aa34–166 of human CD79A. Mouse CD79A BAC DNA was isolated from RP23–80P21, RP23–284H16 bacteria and transformed into pGS1783 cells. The human CD79A fragment, aa34–166 (Fig 1C), was amplified from human genomic DNA using primers:

5’ACGGTACCTGGATGCACAAGGTCCCAGCATCAT3’;

5’TGAATTCATTGAAGACACCCCCTGGGCTCAGCG3’.

The resulting fragment was digested with KpnI and EcoRI and cloned into the PL452 (loxP-Neo-loxP; G418 selection) vector, digested with the same enzymes. The fragment containing hCD79A-loxP-Neo-loxP was amplified using primers:

5’ACCCATCTGTCTCCTCTCCTCTCTCCACAGGTCCCGGATGCCAGGCCCTGTGGATGCACAAGGTCCCAGCA3’;

5’GAGGACACACCTTCTTCCCTTGTCTTGGCTGCATTTGCAGGGGACTCCCGATAACTTCGTATAGCATACATTATACGAAGTTATATTAAGGGTTCCGCAAG3’.

The resulting PCR product was digested with DpnI and electroporated into pGS1783-RP2380P21 cells. A fragment containing pGK-DTA (negative selection in ES cells) was amplified from the pBSKS vector using the following primers:

5’ACATCGGGCAAAACTTATCACTCCTATCTGCCTCTTTCTTTCTAACCCACCGGGTAGGGGAGGCGCTTTTCCCA3’;

Author Manuscript Author Manuscript Author Manuscript Author Manuscript

5’GGAGTGGAGCTGGACGCAAAGGCGGCCTCTGGCTCGGCTAGAGCGACTCTATC GATGAATTCCTGCAGCCCGGGGGATCC3’.

The resulting PCR product was digested with DpnI and electroporated into pGS1783-RP23–80P21-hCD79A-loxP-Neo-loxP cells. The final construct was sequence verified, maxi prepped, linearized with ClaI and, purified for ES cell targeting.

### Chimeric CD79B construct design

In order to generate mice expressing human-mouse chimeric CD79B (cCD79B), targeting constructs were designed in which aa29–153 of mouse CD79A were replaced by aa29–154 of human CD79B. The human CD79B fragment, aa29–154 (Fig 1C), was amplified from human genomic DNA using primers:

5’GCCAGATCGGAGGACCGGTACCGGA3’;

5’TCTGCTTCAGCTGTGCCAAGGTGCT3’.

The resulting PCR product was cloned into the pCR8/GW/TOPO vector. A fragment containing EPKanS was amplified using primers:

5’TCAGTCGACCCCCTCCCTGCATGACTTCCCTCTATCATCCCCCTCTTCCCTCCTG CAGGTCGATTTATTCAACAAAGCCACG3’;

5’TCAGTCGACCGCGTATATCTGGCCCGTACATCG3’.

The resulting product was digested with SalI and cloned into pCR8/GW/TOPO-hCD79B, also digested with SalI. Mouse CD79B BAC DNA was isolated from RP23–386O11, RP23–141A4 bacteria and then transformed into pGS1783 cells. A fragment containing hCD79B and EPKanS was amplified using primers:

5’ACCTAGCCCTGCCCACTTCCTTCCACCCTCCAGGTGAGCCGGTACCAGCAGCCA GATCGGAGGACCGGTACCGGA3’;

5’GATGATGAGGAGGGTCTGGATCAAGATAATGCCATCTTTCAGTGTGTTCCTCTGC TTCAGCTGTGCCAAGGTGCT3’.

The resulting PCR product, containing the Kan/I-SceI insert, was electroporated into pGS1783-RP23–386O11 cells. The Kan/I-SceI selectable marker was then removed from the mutant BAC DNA. A fragment containing loxP-PGK-Neo-loxP was amplified using primers:

5’CCCAGTCCCTGCAGGAGGGAAGAGGGGGATGATAGAGGGAAGTCATGCAGAAG CTTATAACTTCGTATAATGTATGCTATACGAAGTTATTAGGTCTGAAGAGGAG3’;

5’GGCCAAATTCCTAGTCTGTCAACTGAGACCTTCCTCAGTCGACCCCCTCCATAA CTTCGTATAGCATACATTATACGAAGTTATATTAAGGGTTCCGCAAG3’.

Author Manuscript Author Manuscript Author Manuscript Author Manuscript

The resulting PCR product containing loxP-PGK-Neo-loxP was electroporated into pGS1783-RP23–386O11-hCD79B cells. A fragment containing pGK-DTA was amplified from vector pBSKS using primers:

5’GAGCACCCGACTTCTTTTCCAAAGGTCCGGAGTTCAAATCCCAGCAACCACGG GTAGGGGAGGCGCTTTTCCCA3’;

5’TTTAAAAGCAGCTATAAAGTTGGGCTGGGCATGGTCACTCACAGCTGTATATCGA TGAATTCCTGCAGCCCGGGGGATCC3’.

The resulting PCR product containing pGK-DTA was electroporated into pGS1783-RP23–386O11-hCD79B-loxP-PGK-Neo-loxP cells. The final construct was sequence verified, maxi-prepped, linearized with ClaI and, purified for ES cell targeting.

## Embryonic stem cell targeting, blastocyst injection, and germline transmission

JM8A3 ES cells [19] were used for independent targeting of cCD79A and cCD79B constructs. Successfully targeted ES cells were selected using neomycin and screened to identify positive homologous recombinant clones using the Loss of Allele technique as previously described [20]. Putative positive clones were independently verified by LR-PCR (Mouse Genetics Core Facility) and by sequencing (Cambier Lab). Positive ES cell clones were injected into blastocysts to create chimeras. The resulting chimeras were bred with C57BL/6J wildtype mice to establish germline transmission.

## Neo cassette removal and establishing cCD79 homozygosity

In order to remove the loxP-Neo-loxP selection cassette, cCD79A and cCD79B mice were crossed with B6.C-Tg(CMV-cre)1Cgn/J (CMV-cre) (Jackson). Resulting mice were PCR screened for cre-recombination and cCD79 targeting with the following primers:

cCD79A Cre: 5’CTTGGGAGAATGAAAGCACCCACCA3’;

5’TGAGTTCAAGGCCAGCCAGGGCTA3’

CD79A Forward: 5’GGTACGGCTCCACTCCTGATG3’;

hCD79A reverse: 5’CATTCTGGATGATCAGCGTAC3’;

mCD79A reverse: 5’GTGCTGCTCAGCATTCTGGTG3’.

cCD79B Cre: 5’GTGCTCACTAAGAACAAGGCAGTCG3’;

5’CTGCACAGGCTTGAAATCCTCAGTC3’;

CD79B Forward: 5’CGGAAGGAGGAAGTAGCTCTG3’;

hCD79B reverse: 5’CCTTCAGTGGCCAAGGCTGGA3’;

mCD79B reverse: 5’ATCCTTAGCCTGTCACCCGAG3’.

Author Manuscript Author Manuscript Author Manuscript Author Manuscript

Mice positive for CD79A and CD79B cre-recombination generated PCR bands at 322bp and 254bp, respectively. Positive targeting of cCD79A and cCD79B knock-in sequences generated bands at 303bp and 387bp, respectively. Wildtype mCD79A and mCD79B generated bands at 590bp and 524bp, respectively. Non-agouti (i.e. black), cre-recombined mice heterozygous for cCD79A or cCD79B were crossed in order to generate singly homozygous mice expressing cCD79A or cCD79B. To ensure accurate targeting of the cCD79, cDNA was purified from homozygous cCD79A or cCD79B knock-in mice and sequenced using the following primers:

cCD79A PCR: 5'ACGGCTGAACAGGAAGTGAG3';
5'AGGGATGCTGGAGTCAGACA3'.

cCD79A sequencing: 5'CTGGTACCTCAAGGCTACGG3';

cCD79B PCR: 5'TCCTTGGGCTCAGAGACAGA3';
5'TGATGGTCCAGCTTCAGACG3';

cCD79B sequencing: 5'GCCCAACAGTTGAGCAGGAT3'.

Transcription of the chimeric CD79 molecules in B cells was first confirmed via PCR analysis of splenic B cell-derived cDNA followed by alignment of sequences with those of the targeting constructs. Singly homozygous mice expressing cCD79A and cCD79B were intercrossed to generate the cCD79A/B doubly homozygous mouse.

## Generation of anti-human CD79 antibodies

Details about the generation of humanized anti-human CD79 antibodies can be found in the United States Patent Application 20200109198, Anti-CD79 Antibodies and Their Uses [21]. In order to generate the surrogate mouse anti-human CD79 antibody [Curly-14], mice were immunized with human CD79 fusion proteins. The extracellular, immunoglobulin-like domains of human CD79A and B, joined by a peptide linker, were expressed via baculovirus and fused to a FLAG tag (Sigma-Aldrich). After expression in Sf9 cells, protein was purified using an anti-FLAG gravity-column packed with anti-FLAG resin (Sigma). Human CD79 fusion protein was eluted in buffer containing 0.01% sodium azide, PBS, and competing FLAG peptide (Sigma). The mouse deemed "Curly" was immunized IP with hCD79 in complete (CFA) and incomplete (IFA) Fruend's adjuvant according to the following schedule: d0, CFA + 50 μg hCD79; d14, IFA + 50 μg hCD79; d24, serum tested for binding to hCD79 by ELISA; d136, IFA + 50 μg hCD79; d199, IFA + 60 μg hCD79; d270 50 μg hCD79 in PBS. On d273, after this immunization regimen, Curly was sacrificed and fused using standard hybridoma procedures [22]. Curly-14 was humanized, mutated, and affinity matured, generating the anti-human CD79A clinical candidate. Human IgG4 anti-human CD79A antibodies contain the S228P mutation to stabilize the hinge region and prevent VL Fab arm exchange. In addition to S228P, antibodies were produced with either the D265A or F234A/L235A ("FALA") mutations to reduce effector function. Experiments presented here were performed with the hIgG4 S228P/D265A anti-human CD79A variant. Anti-human CD79 antibodies were provided by Panorama (huIgG4) and Biogen (humanized VH/VL

Author Manuscript Author Manuscript Author Manuscript Author Manuscript

chimerized to murine IgG1 bearing N297Q agly mutation as reduced effector function murine surrogate or mIgG2a as effector-competent comparator).

### PBMC isolation

Peripheral blood mononuclear cells were purified using cell prep tubes (Vacutainer, CPT) according to the manufacturer's protocol (BD, 362753).

### Mice

Unless otherwise noted, 8–16-week-old male and female mice expressing chimeric (c) CD79 (cCD79A; cCD79B; cCD79AB) were used in all experiments. No differences were observed between males and females of any of the three genotypes. Control female, age-matched, wild type C57BL/6J mice were purchased from The Jackson Laboratory. Formal nomenclature and informal names include C57BL/6-human CD79AB chimeric mice and ch-hCD79AB or cCD79AB mice, respectively.

### Tissue harvesting and B cell isolation

Genomic DNA was prepared from ear clips for PCR and sequence analysis. A 1–2 mm ear notch is placed in 50 μL alkaline lysis reagent (25 mM NaOH, 0.2 mM EDTA, pH ~12) and incubated at 95°C, overnight, before neutralizing with 50 μL of 40 mM Tris-HCl, pH ~5. Lymphocytes were prepared for analysis by multiple means. Spleens and bone marrow were harvested in IMDM supplemented with 5% FCS, 1 mM sodium pyruvate, 50 μg/mL gentamicin, 100 U/mL pen/strep, 2 mM l-glutamine, and $5 \times 10^{-5}$M beta-mercaptoethanol; single cell suspensions were prepared by mechanical disruption. RBCs were lysed with 1 mL of ACK (150 mM $NH_4Cl$, 10 mM $KHCO_3$, and 100 mM $Na_2EDTA$) for 1 min at room temperature (RT). Cells were subsequently washed and resuspended in complete medium.

For B cell isolation, spleen cells were harvested, RBC depleted by ammonium chloride tris lysis, and resuspended in 1 mL medium together with 40 μL of anti-CD43 Microbeads (Miltenyi Biotech) per mouse per spleen. The cell/bead mixture was rotated while incubating at 4°C for 10 minutes. LS MACS separation columns (Miltenyi Biotech) were washed with 5 mL medium. The cell/bead mixture was flowed over the column, which was then washed with 5 mL medium while collecting the flow-through. These preparations were routinely >95% B cells. Serum was prepared from peripheral blood collected from the tail vein.

### Flow cytometry

Cells were resuspended at 1E7 cells/mL in cold FACS buffer (1% BSA in PBS) containing 0.1% sodium azide ($NaN_3$). Then, 100 μL aliquots containing 1E6 cells were stained with fluorochrome conjugated monoclonal antibodies. After staining for 1 hour in the dark at 4°C, cells were washed twice and resuspended in 300 μL FACS buffer. Data was acquired on a Fortessa X-20 flow cytometer (Becton Dickinson) and analyzed with FlowJo software.

For intracellular detection of phospho-Syk and PTEN, splenocytes were collected from mice that had received 250 μg IP injections of either control human IgG4 [VLN3G2], reactive with an irrelevant human carcinoma antigen, or human IgG4 D265A anti-human CD79A

Author Manuscript Author Manuscript Author Manuscript Author Manuscript

24 hours prior to harvest. Cells were rested at 37°C in serum-free medium for 1 hr. To measure BCR-mediated induction of Syk phosphorylation, 1E6 splenocytes in 1 mL serum-free medium were stimulated for 5 minutes with 10 μg/mL goat $F(ab')_2$ anti-mouse IgM (JacksonImmuno). To ensure that there were no interactions between antibodies, both resting and stimulated cells were centrifuged at 4500 rpm for 20 sec before aspirating supernatant and resuspending in 100 μL of fixation buffer (BD, Cytofix) for 20 min at 4°C. Cells were washed 3 times in FACS buffer before being stained with fluorescent fab anti-mIgG (H+L) and anti-B220. After staining cells were washed 3 times in permeabilization buffer (BD, Cytoperm). Rested and stimulated cells were then stained with anti-pSyk (Y352) or isotype control antibodies in 50 μL permeabilization buffer. Rested cells were stained with anti-PTEN or isotype control. Cells were washed and data was collected as described above.

## Antibodies

Bone marrow, peripheral blood, and splenic B cells from cCD79 and wild type mice were analyzed using the following antibodies: hCD79A-PE (R&D Systems, FAB69201P); hCD79B-PE (abcam, ab33295); mCD79B-AF488 ([HM79], made in house); hCD79A-AF647 ([Curly-14], made in house); B220-BV786 (BD, 563894); B220-APC (BD, 103212); B220-PE (BD, 561878); CD43 ACP-Cy7 (BD, 562866); BP1-PE (BD, 553735); CD24-APC (BioLegend, 101814); IgD-FITC (BioLegend, 405704); IgM-BUV396 (BD, 564025); CD19-FITC (BioLegend, 152404); CD93-APC (BioLegend, 136510); CD23-FITC (BD, 561772); CD1d-PE (BD, 553846); CD95-PE (BD, 554258); GL7-FITC (BD, 553666); fab anti-mIgG (H+L)-AF647 (Jackson ImmunoResearch, 115–606-072); phospho-Syk (Y352)-PE (BD, 557881); PTEN-PE (BD, 560002); mouse IgG1 isotype control-PE (BD, 559320).

## Immunohistochemistry

Spleens were flash frozen in tissue casts on dry ice containing OCT embedding medium (Tissue-Tek) and stored at −80°C until sectioning. 6 μm sections were cut using a cryostat and thaw-mounted on super frost plus glass slides (Fisher), that were then air-dried for 3 hours at RT and stored at −80°C. Frozen sections were fixed in ice-cold acetone for 5 minutes, air-dried, rehydrated with PBS and then blocked for 20 minutes with PBS + 5% FCS. Blocking buffer was aspirated and sections were stained for 2 hours in 100 μL PBS containing fluorescent antibodies. B cells were detected with B220-PE (Pharmingen). CD4 T cells were detected with CD4-Cy5 (Caltech). Slides were washed twice before being mounted in fluoromount G. Images were recorded on a Nikon Eclipse TE2000-E fluorescence microscope and further analyzed with Slidebook 6 software.

## SRBC immunizations

Mice were immunized with sheep red blood cells in accordance with standard procedures [23]. 1 mL citrated sheep's blood (Colorado Serum) was washed two times in 50 mL PBS and then resuspended 1:10 in PBS. Mice received 100 μL IP of this 0.1% suspension. Spleens were harvested at d5 post immunization and B cells were assayed for germinal center markers (CD95, GL7).

Author Manuscript Author Manuscript Author Manuscript Author Manuscript

## Immunoblotting

Isolated B cells were resuspended in serum-free medium and allowed to rest at 37°C for 30 minutes. 4E6 B cells in 1 mL serum-free medium were stimulated for 5 minutes with 10 μg/mL rabbit $F(ab')_2$ anti-mouse IgG (H+L) (Jackson ImmunoResearch, 315–006-003). Stimulated cells are centrifuged at 4500 rpm for 20 seconds before aspiration of medium and addition of 30 μL lysis buffer (NP-40 + inhibitors (PMSF, protease inhibitors, $NaVO_3$, NaF)). Cells were suspended by vortexing and incubated on ice for 10 minutes. After centrifugation of whole-cell lysates for 15 minutes, 13,000 rpm, 4°C, the supernatants were collected and to 30 μL, 10 μL of 4X reducing SDS loading buffer was added. Samples were then boiled at 100°C for 10 minutes and stored at −20°C until use.

Samples were thawed in boiling water before being loaded into a 10% SDS-PAGE Tris-HCl gel. Current was applied for approximately 1.5 hours at 110V until the dye front reached the bottom of the gel. The separated proteins were then transferred to a PVDF membrane using a semi-dry transfer apparatus and transfer buffer (25 mM Tris pH 7.5, 192 mM Glycine, 20% methanol and 0.05% SDS). The transfer was run for 1.5 hours, 25V, and 0.15 amp per gel.

Protein-transferred membranes were blocked in Odyssey blocking buffer (Licor) while rocking overnight at 4°C. The next day primary antibodies against intracellular signaling molecules, i.e. phosphotyrosine [4G10]-AF647, actin (Santa Cruz, sc1616), pSyk (Cell Signaling, #2711), pIga (Cell Signaling, #5713), and affinity purified polyclonal rabbit antibodies made in-house including anti-Syk, mouse CD79B cytoplasmic tail, and mouse CD79 extracellular domains were added in blocking buffer and incubated for 2 hours while rocking at RT. After washing membranes 3 times in TBS + 1% Tween for 10 minutes each, fluorochrome-conjugated secondary antibodies, donkey anti-goat IgG IR800 (Licor), goat anti-rabbit AF680 (Life technologies), or SA-AF647 (made in house) were added in blocking buffer and incubated for 2 hours while rocking at RT. Membranes were washed 3 more times before being imaged on the Odyssey (Licor). Image studio software (Licor) was used to quantify western blot band densities.

## Measurement of intracellular free calcium ($[Ca^{2+}]_i$)

For measurement of relative intracellular free calcium concentration ($[Ca^{2+}]_i$), RBC-depleted splenocytes (1E7/mL in complete medium containing 2% FCS) were stained with anti-B220 and Fab anti-mouse IgG (H+L), while being loaded with 5 μM indo-1 acetoxymethyl ester (INDO-1 AM, Thermofisher) according to the manufacturer's protocols. Both Indo loading and flow cytometry were performed at room temperature (RT; ~22°C). After being washed once in medium, cells were resuspended at 5E6 cells/mL in RT medium in 500 μL aliquots. Indo-1 was excited with a 355 nm UV laser, and $Ca^{2+}$-bound indo-1 was detected with a 379/28 bandpass filter; unbound indo-1 was detected with a 524/40 bandpass filter. Induced changes in relative intracellular free calcium concentration ($[Ca^{2+}]_i$) was determined by calculating the ratio of $Ca^{2+}$ bound/unbound indo-1 signals over time. After data were acquired for 30 s to establish $[Ca^{2+}]_i$ baseline, cells were stimulated with the indicated dose of goat $F(ab')_2$ anti-mouse IgM, rabbit $F(ab')_2$ anti mouse IgG (H+L), goat $F(ab')_2$ anti-human IgM Cμ5, or rat anti-mouse IgM [B-7–6]

Author Manuscript Author Manuscript Author Manuscript Author Manuscript

(JacksonImmuno) and data were collected for an additional 2 min 30 s. The relative $[Ca^{2+}]_i$ was measured using a Fortessa X-20 flow cytometer and analyzed with FlowJo software.

### Nitrophenyl-conjugated ovalbumin immunizations

To prepare the immunogen, a 1:1 volume mixture of 1 mg/mL $NP_{4.5}$OVA (Biosearch Technologies) and 10 mg/mL alum (Serva; Alu-Gel-S) was incubated, while rotating, for 3 hours at RT. A total of 200 μL of the mixture was injected IP per mouse in order to achieve immunization with 100 μg $NP_{4.5}$OVA and 1 mg alum.

### NP-ficoll immunizations

Mice were injected IP with 25 μg $NP_{59}$-ficoll (Biosearch Technologies) in 200 μL PBS. Spleens were harvested on d7 post immunization for analysis of NP-specific, $IgM^+$ antibody secreting cells.

### Measurement of IgM, IgG, NP-specific IgG, and Chromatin-specific IgG

Enzyme immunoassay/RIA 96-well plates (Corning, CLS3590) were coated with 50 μL of 20 μg/mL $NP_{20}$BSA or $NP_2$BSA (Biosearch) or 1 μg/mL goat anti-mouse IgG or goat anti-mouse IgM (Southern Biotech) in ELISA capture buffer (PBS + 150 mM NaCl). For detection of anti-chromatin IgG, plates were coated using 50 μL of 10 μg/mL calf chromatin (Larry Wysocki, National Jewish Health) in ELISA buffer containing 1mM EDTA. Plates were incubated overnight at 4°C. The following day, wells were aspirated, blocked with 2% BSA in PBS, and incubated overnight at 4°C. Serum was added and serially diluted in 3-fold increments across the plate. The initial serum dilutions used were 1:500 for total IgM, 1:1000 for total IgG, and 1:200 for NP-specific IgG. For detection of IgG anti-chromatin, serum was diluted 2-fold down the plate starting at a serum dilution of 1:20. Plates were incubated overnight at 4°C before being washed 3 times with PBS + 0.05% Tween. Secondary antibodies, for respective detection, were added in 100 μL 1% BSA in PBS + 0.05% Tween. These antibodies include: goat anti-mouse IgG1-HRP (Southern Biotech), goat anti-mouse IgG-HRP (Southern Biotech), or goat anti-mouse IgM-HRP (Southern Biotech). After overnight incubation with secondary antibodies, wells were washed and 50 μL TMB single solution (Life Technologies) was added for 5 min. Wells were quenched with 50 μL 1M $H_2SO_4$ before recording absorbance at 450 nm.

### NP-specific ELISPOT

ELISPOT plates were prepared as above. For ELISPOT analysis, serial 2-fold dilutions of 1E6 splenocytes/ 100 μL sample were plated in triplicate. Cells were allowed to settle to the well bottoms while tapping the edges of the plate. Plates were incubated at 37°C for 6 h, then washed 3 times, for 10 min each, with PBS + 0.05% Tween. Next, 50 μL secondary goat anti-mouse IgG-AP or IgM-AP (Southern Biotech) in 2% BSA PBS was added and incubated overnight at 4°C. After washing 3 times in 0.05% Tween PBS, plates were incubated with ELISPOT development buffer (25 μM (BCIP) 5-bromo-chloro-3-indolyl phosphate p-toluidine, 100 mM NaCl, 100 mM Tris, 10 mM $MgCl_2$ [pH 9.5]) for 1 h. The reaction was stopped by washing plates 3 times with tap water and 1 time in di

Author Manuscript Author Manuscript Author Manuscript Author Manuscript

water. The number of spots at a cell dilution was determined. The frequency of NP-specific antibody-secreting cells (ASCs) was calculated based on spot counts within the linear range.

### Tetanus toxoid (TT) antibody secreting cell ELISPOT

Detection of antigen-specific B cells was carried out as previously described [24]. Briefly, PBMCs were collected from consenting volunteers at 7–10 days post boost with tetanus, diphtheria, and pertussis vaccine (Tdap). 5E6 PBMCs were incubated overnight in 1 mL medium containing 25 μg of either hIgG4 D265A anti-hCD79A, mouse anti-hCD20 (Panorama), or control hIgG4. Following overnight incubations, cells were washed, counted, and loaded on to ELISPOT plates that had been previously coated with tetanus-toxoid (100 μL at 10 μg/mL). Cell suspensions were diluted two-fold across the plate starting with 1E6 cells in the first column. After 6-hour incubation, plates were washed, and antibody secreting cells were detected with biotinylated anti-human IgG (H+L) and streptavidin-AP. ELISPOT plates were further developed and analyzed as described above.

### Pristane induction of autoantibody formation

Female and male cCD79A knock-in mice, aged 8–12 weeks, were injected IP with 500 μL of pristane (Sigma-Aldrich) on day 0. Weekly injections (250 μg, IP) of either human IgG4 anti-human CD79 D265A or isotype control human IgG4 [VLN3G2] (ATCC, HB-8636) were given on d0, 7, 14, 21, 28, 35, 42, 49, and 56. Sera was collected for anti-chromatin autoantibody analysis prior to any injections and on d30, 50, and at the conclusion of the experiment at d64. Pooled sera from diseased SLE1.2.3 mice (Raul Torres, CU) and serum from wild type C57BL/6 were used as positive and negative controls, respectively, in IgG anti-chromatin assays.

### Experimental autoimmune encephalomyelitis (EAE)

EAE was induced by following standard protocols [25]. All reagents, including antibodies, for this experiment were provided by Biogen. Serum ELISAs and spleen flow cytometry were also performed at Biogen. Briefly, 16-week-old male and female cCD79A$^{+/+}$B$^{+/-}$ mice were immunized SC with 50 μg human recombinant myelin oligodendrocyte glycoprotein (hMOG$_{1–125}$) emulsified in 200 μg complete Freund’s adjuvant (CFA) on d0. Mice also received IP injections containing 200 ng pertussis toxin in PBS on d0 and d2. Weekly antibody injections were given on d-3, 4, 11, 18, and 25, relative to immunization with hMOG. Treatment arms were blinded, only to be revealed after mice had received scores for the duration of the experiment. Mice received 20 mg/kg IP injections of either mIgG2a anti-hCD79, mIgG1 aglycosylated anti-hCD79, or anti-HEL isotype controls. Mice were weighed and scored daily using a 5-point scale (0= no disease, 1= complete tail paralysis, 2= hind leg weakness, 2.5= complete paralysis of 1 hind limb, 3= complete bilateral hind leg paralysis, 4= front limb weakness with complete bilateral hind limp paralysis, 5= Complete bilateral hind- and fore-limb paralysis, moribund, or dead.) Sera were collected on days −7, 15, 22, and 30 for analysis of anti-MOG IgG and phosphorylated neurofilament heavy chain (pNfH). At takedown on d30, spleens were harvested to measure B cell depletion, IgD expression, and other immune cells. Spinal cords were also harvested for histological examination of disease pathology.

Author Manuscript Author Manuscript Author Manuscript Author Manuscript

For detection of anti-MOG autoantibodies, serum samples were diluted 1:5000 in casein blocking buffer before loading 100 μL on to plates that had previously been coated with 100 μL of 1.0 μg/mL recombinant mouse MOG (R&D Systems, 8536-MO-050). After incubation and washing, anti-MOG antibodies were detected with goat anti-mouse IgG-HRP followed by TMB substrate. Plates were developed for 5–10 minutes before quenching with 1.0N sulfuric acid solution and reading plates at 450 nm.

Neurofilament assays were run as follows: Briefly, sera were thawed on ice then diluted 1:6 by adding 12 μl serum to 60 μl dilution reagent from the Simple Plex Human NF-H Cartridge (ProteinSimple, SPCKB-PS-000519) in a V-bottom 96-well plate. 50 μl of each sample was then loaded into the sample wells of the cartridge, the plate was prepared with wash buffer as per the protocol, then run on the Biotechne (ProteinSimple) Ella Automated Immunoassay System (Prod# 600–100).

For flow analysis of spleen cells, RBC-lysed splenocytes were suspended at 5E6 cells/mL and fixed by adding 0.5 mL of 6% PFA to 1 mL splenocytes. After a 20-minute fixation, cells were washed and frozen. Thawed samples were resuspended in FcR-block (BD Biosciences, 553142) prior to staining with the following antibodies: CD45-AF488 [30-F11] (Biolegend #103122), CD8a-PerCP Cy5.5 [53–6.7] (Biolegend #100734), CD4-BV421 [GK1.5] (Biolegend #100443), CD19-APC [1D3] (Biolegend #152410), B220-BV785 [RA3–6B2] (Biolegend #103246), Ly6G-AF700 [1A8] (Biolegend #127622), Ly6C-BV605 [HK1.4] (Biolegend #128035), CD11b-PE [M1/70] (Biolegend #101208), IgD-BV510 [11–26c.2a] (BD Biosci #563110). Data were acquired on a Bio-Rad ZE5 flow cytometer and analyzed using FlowJo software.

## Tamoxifen induction of PTEN knock-out

B cell specific knock-out of PTEN was achieved with a single IP injection of 2 mg tamoxifen, dissolved in corn oil, into hCD20-Cre$^{TAM}$ X ROSA26-STOPflox-YFP X *PTEN*$^{flox/flox}$ or control hCD20-Cre$^{TAM}$ X ROSA 26 STOPflox YFP X *PTEN*$^{WT}$ mice [26]. On day 7 post tamoxifen, mice are injected with anti-CD79 or isotype control antibodies. After 18 hours, YFP$^{+}$ B220$^{+}$ splenic B cells are analyzed on PTEN expression, antibody coating, and BCR mediated calcium mobilization.

## Statistical analysis

GraphPad Prism software was used to generate graphs and perform statistical tests. Unless otherwise noted, statistical significance was calculated by student's t-test in order to make pairwise comparisons between control and experimental groups as well as between experimental groups. For statistical analysis of EAE disease scores and time to EAE onset, Kruskal-Wallis with Dunn's multiple comparison test and Wilcoxon Log-Rank test were employed, respectively. ns, not significant; *, $p<0.05$; **, $p<0.01$, ***, $p<0.001$; ****, $p<0.0001$.

Author Manuscript Author Manuscript Author Manuscript Author Manuscript

## Results

### B cells in chimeric human-mouse CD79 knock-in mice express fully functional chimeric antigen receptors and undergo normal development.

To develop mice expressing extracellular human CD79 domains, the immunoglobulin-like domains of mouse CD79 were replaced by genomic DNA knock-in of human homologues, independently creating chimeric CD79A and chimeric CD79B (cCD79A and cCD79B, respectively) mice (Fig 1C).

The rationale for construction of chimeric CD79 mice is as follows: epitopes recognized by anti-human CD79 antibodies must be expressed without disturbing the signaling capacity of mouse BCRs. Therefore, we replaced only the extracellular portions of mouse CD79 A and B molecules. Conserved cysteines, and therefore the supportive disulfide bridges, are maintained in the extracellular Ig-like domains of human and mouse CD79A and B. This suggests that heterodimer pairings of chimeric CD79 with endogenous mouse CD79 proteins should be expressed on the cell surface. This was an important consideration due to the fact that cCD79A and cCD79B knock-in mice were made independently, later to be interbred to create doubly homozygous cCD79AB animals. High conservation of mouse and human transmembrane domains suggest uninterrupted association of the chimeric CD79 with mouse immunoglobulin in B cell plasma membranes [27]. Cytoplasmic domains containing immunoreceptor tyrosine-based activation motifs (ITAMs) are entirely mouse derived. Therefore, interaction of cCD79 with intracellular signaling effectors should be intact. Thus, we hypothesized that these constructions would allow cCD79 binding of anti-human CD79 antibodies while preserving interactions among mouse CD79 chains and membrane-bound immunoglobulin. Further, cCD79 should interact faithfully with downstream signaling intermediaries. The former interactions are critical for BCR transport to and expression on the cell surface and the latter for BCR signaling, both required for B cell development and function.

Before engaging in the study of the effects of candidate anti-human CD79 therapeutics, it was important to verify normalcy of cCD79 expression, association with murine partners, and function in B cell development and antibody responses. Knock-in mice homozygous for cCD79A, cCD79B or cCD79A and B were observed to be viable, fertile, and develop normally with no grossly apparent signs of developmental defect nor immunodeficiency. As depicted in the first two columns of figure 1D, anti-human CD79A [706931] is reactive with cCD79A and cCD79AB mice, but not fully murine CD79 nor cCD79B mice. Conversely, anti-human CD79B [AT105–1] stained B cells from cCD79B and cCD79AB mice, but not fully murine CD79 nor cCD79A mice. B cells from cCD79A mice also stained with the mouse anti-human CD79 [Curly-14] and the previously described hamster anti-mouse CD79 [HM79] allowing assignment of their specificities for hCD79A and mCD79B, respectively. Intensity of staining further suggests that the epitope recognized by Curly-14 is contained entirely within the A chain of human CD79. Importantly, the cCD79A homozygous mouse conveniently allows head-to-head comparison of biological effects of the anti-mouse CD79B and the anti-human CD79A clinical candidate in the same cell.

Author Manuscript Author Manuscript Author Manuscript Author Manuscript

Loss of the extracellular portions of mouse CD79 proteins was confirmed by immunoblot analysis of whole cell lysates (Fig 1E). B cells ($CD43^{-}$) from the spleens of cCD79 and wild-type mice were lysed and subjected to protein fractionation by SDS-PAGE followed by transfer to PVDF membranes. Protein-adsorbed membranes were probed with polyclonal rabbit antibodies recognizing mouse CD79. The upper panel was blotted with affinity purified polyclonal rabbit antibodies reactive with Sf9-expressed mouse CD79AB extracellular domain heterodimers. Bands representing mouse CD79A (~34kD) and B (~37kD) are seen in WT B cell lysates. As seen in the cCD79A lane, the rabbit anti-mCD79AB recognizes mCD79B but does not recognize human CD79A. Similarly, this polyclonal antibody does not recognize human CD79B when expressed as a heterodimer with WT mCD79A, or a heterodimer of cCD79A. The middle panel shows the membrane blotted with polyclonal rabbit antibody raised against the mouse CD79B cytoplasmic domain, the sequence of which is found in both mCD79B and cCD79B, illustrating equivalent lane loading. These data, together with the B cell staining in figure 1D, suggest not only successful expression of chimeric receptors but also successful paring of chimeric and endogenous mouse CD79 molecules. The presence of B cells in the spleens of cCD79 mice is also suggestive of successful selection, egress from the bone marrow and survival in the periphery. These observations further demonstrate a lack of polyclonal rabbit antibody cross-reactivity between mouse and human CD79A and B extracellular domains.

To further examine *in vivo* co-expression of chimeric and mouse CD79, we analyzed B cell surface staining in animals homozygous at cCD79A containing 0, 1 or 2 copies of the cCD79B encoding gene. Staining of $CD19^{+}$ human PBMCs by anti-human CD79B [AT105] was first confirmed (Fig 1F), before co-staining cCD79 B cells with anti-mouse CD79B [HM79] (Fig 1G). $cCD79A^{+/+}cCD79B^{+/-}$ B cells stained positively for both mouse and human CD79B, with intensities consistent with cCD79B gene dose. This suggests similar efficiency of cCD79A pairing with either mCD79B or cCD79B. However, mouse CD79B appears to be favored slightly in pairing with the chimeric CD79A, as shown by dual staining of mouse CD79B and human CD79B in $cCD79A^{+/+}B^{+/-}$ cells (Fig 1G). This is suggested by off-diagonal staining of mouse CD79B. This finding is consistent with reduced signal seen in figure 1D, i.e. in some B cells hCD79A staining is reduced in cCD79AB B cells relative to cCD79A animals. In contrast, gain of hCD79B staining and coincident loss of mCD79B further demonstrates near equivalent pairing and expression of both chimeric and mouse CD79 proteins. Near equivalent surface levels of both IgM and IgD on B cells from these genotypes suggests that there is no defect in BCR expression as a consequence of pairing of chimeric and mouse CD79 chains (Fig 1H).

Taken together, these data demonstrate successful generation of the chimeric human-mouse CD79 extracellular domain knock-in mice. Further, the ability to detect nearly normal expression of the cCD79 molecules, and identical expression of IgM and IgD, demonstrate effective pairing and suggest no defect exists in B cell development and maturation as a consequence of CD79 extracellular domain swapping. Formal analysis of B cell development is described in supplemental figures 1–4. Briefly, no significant deviations in B cell developmental populations in the bone marrow (i.e. Hardy fractions) nor peripheral B cell populations in the spleen were observed in cCD79 mice as compared to C57Bl/6 wild-

Author Manuscript Author Manuscript Author Manuscript Author Manuscript

type animals (Supplemental Fig 1–3). Additionally, B cell activation *in vivo* and steady-state serum Ig concentrations are unaffected by expression of cCD79 (Supplemental Fig 4).

### Expression of cCD79 does not affect BCR signaling function.

Data presented thus far suggest function of the murine BCR is unaffected by replacement of CD79A and B extracellular domains with their human counterparts; B cell development and survival are dependent on surface expression and tonic BCR signaling [28] [29] [30]. In order to properly assess effects of cCD79 on BCR signaling we measured tyrosine phosphorylation of membrane-proximal signaling effectors and calcium mobilization following receptor stimulation.

Initial steps in BCR signaling include the tyrosine phosphorylation of Lyn, Syk, Btk, PLC$\gamma$ and, most proximally, CD79 receptor components on which conserved tyrosine residues in ITAMs are phosphorylated to initiate downstream signaling [31]. Phosphorylation of these signaling intermediaries propagates the BCR signal leading to the eventual activation of the B cell. In order to assess total BCR-mediated tyrosine phosphorylation in cCD79 animals, we prepared whole-cell lysates of splenic B cells that had been stimulated *in vitro*. B cells from wild-type and cCD79 animals were purified by CD43 negative selection and subjected to BCR stimulation with $F(ab')_2$ fragments of rabbit anti-mouse Ig containing reactivity to heavy chains and light chains (H+L), and therefore reactive with all BCR. Whole-cell lysates from stimulated B cells were fractionated by SDS-PAGE and transferred to PVDF membranes which were subsequently blotted with phosphotyrosine/context-dependent antibodies, i.e. pTyr (Fig 2A), pCD79A (Fig 2B) and, pSyk (Fig 2C). Whole-cell lysates from resting cells demonstrate equivalent levels of basal phosphorylation. Membranes were re-probed with anti-actin, anti-mCD79B or anti-Syk antibodies, respectively, to control for equivalent loading. Images obtained from these blots demonstrate a similar degree of tyrosine phosphorylation in cCD79 B cells compared to wild type. This includes global phosphotyrosine (Fig 2A), phospho-CD79A (Fig 2B) and, phospho-Syk (Fig 2C).

Calcium mobilization, along with parallel activation of other downstream pathways, is important in BCR signaling [32]. Tyrosine phosphorylation leads to activation of PLC$\gamma$, which cleaves phosphatidylinositol 4,5-bisphosphate (PIP2) into diacylglycerol (DAG) and inositol 1,4,5-trisphosphate (IP3). Stimulation of IP3 receptors in the ER membrane initiates release of intracellular calcium stores and this activates entry of extracellular calcium. Ultimately, calcium-dependent nuclear translocation of the transcription factor NFAT contributes significantly to B cell activation. Thus, elevation of $[Ca^{+2}]_i$ in BCR-stimulated cells is a simple measure of complex signaling events that occur proximal to the receptor. In order to assess calcium mobilization in B cells expressing cCD79, we recorded fluorescent emissions of intracellular calcium reporter (INDO-1) before and after stimulation with antibodies recognizing membrane immunoglobulins. Splenocytes from cCD79 and wild-type control animals were simultaneously stained for B cells (B220) and loaded with the calcium-sensing dye. When bound to cytoplasmic $Ca^{2+}$ ions, INDO's emission shifts from 525 (unbound) to 379 nm. A ratio of 379/525 is used as a measure of relative intracellular free calcium level ($[Ca^{+2}]_i$). After 30 seconds of data acquisition, to establish basal $[Ca^{+2}]_i$, cells are stimulated with anti-BCR antibodies (anti- IgM, IgG, etc.) and $[Ca^{+2}]_i$ recorded for

Author Manuscript Author Manuscript Author Manuscript Author Manuscript

an additional 150 seconds. As seen in figure 2D, stimulation of cCD79-containing BCRs results in similar amplitude changes in $[Ca^{2+}]_i$, time to maximal calcium and attenuation of the calcium signal. These observations suggest that circuitry involved in both activation and regulation of BCR signaling is operative in cCD79 B cells.

Taken together, these data demonstrate normal signaling functionality of the BCRs comprising murine immunoglobulins and human/mouse chimeric CD79A and B. To further interrogate BCR function in cCD79 animals, we analyzed B cell antibody responses following immunization.

## WT and cCD79 mice respond equivalently to immunization with thymus-dependent and thymus-independent immunogens.

B cell immune responses to both thymus-dependent and thymus-independent immunogens, as measured by generation of antibody secreting cells (ASC) and serum antibody, reflect a complex orchestration of both inter- and intracellular interactions [33]. In order to test the capabilities of cCD79-containing BCRs to participate in these responses, we first immunized mice IP with $NP_{4.5}$-conjugated ovalbumin, in alum, and measured the primary immune response via ELISPOT and ELISA (Fig 2E and F). At take-down, 16 days after immunization with NP-Ova + alum, we observed equivalent numbers of both total and high-affinity, IgG antibody-secreting cells specific for NP (Fig 2E). Similarly, accumulated IgG antibody in peripheral blood serum of immunized animals was found to be relatively identical between control and humanized animals (Fig 2F). We also measured responses that are independent of T cell help, which rely more heavily on the signaling efficiency of the BCR. To this end we immunized control and knock-in animals with high-avidity $NP_{59}$-conjugated ficoll. Seven days later, near equivalent numbers of IgM anti-NP ASC were seen in all groups of immunized animals (Fig 2G).

In conclusion, in addition to functioning at the level of molecular signaling, activation of $cCD79^+$ B cells results in immune responses that are indistinguishable from wild type animals. Confirmation of B cell functionality in cCD79 expressing animals permitted us to explore the treatment effects of candidate anti-huCD79 therapeutic antibodies *in vivo*. This includes effects of treatment on BCR signaling, immune responsiveness, and modulation of murine autoimmune disease models.

## In vivo treatment with anti-human CD79 antibody induces changes similar to those observed in anergic B cells.

Ultimately, chimeric CD79 mice could serve as an important tool for validation of therapeutic antibodies and CAR-T cells targeting human CD79. Thus, we wished to explore the biologic activity of anti-human CD79A. Both human peripheral B cells ($CD19^+$) (Fig 3A, left) and Ramos cells (Fig 3A, middle) were recognized by the Curly-14 anti-human CD79A antibody. At the same dilution of staining antibody, Curly-14 bound cCD79A B cells, which are dually stained with anti-mCD79B [HM79] (Fig 1D and Fig 3A, right). The mouse anti-human CD79A monoclonal [Curly-14] was further humanized (hIgG4), Fc-mutated (S228P/D265A or S228P/F234A/L235A), and affinity matured in preparation for preclinical analysis. The candidate human IgG4 S228P/D265A anti-human CD79A,

Author Manuscript Author Manuscript Author Manuscript Author Manuscript

referred to as hIgG4 D265A anti-hCD79A, was used for all experiments presented here. This monoclonal was first validated based on its ability to bind cCD79A B cells, *in vivo* (Fig 3B). cCD79A mice were injected IP with 250 μg of either hIgG4 D265A anti-hCD79A, isotype control hIgG4 [VLN3G2], or hamster anti-mouse CD79B [HM79]. After 18 hours, splenic B cells ($B220^+$) were analyzed by flow cytometry for staining with anti-human CD79A [AF647-Curly-14] and anti-human IgG4 (Fig 3B). The first panel of figure 3B shows that previous injection with human IgG4 D265A anti-human CD79A completely blocks binding of Curly-14, the parental anti-human CD79A; neither HM79 nor control hIgG4 blocks Curly-14 binding. The second panel of figure 3B shows coating of B cells with human IgG4 in mice previously injected with hIgG4 D265A anti-human CD79A but not in mice injected with hIgG4 isotype nor HM79. These data confirm that Curly-14's specificity is maintained in the humanized clinical candidate. The first observable *in vivo* effects of the anti-human CD79A clinical candidate are seen at the B cell surface in splenocytes taken from cCD79A mice injected IP with 250 μg of antibody 18 hours prior (Fig 3C). In comparison to hIgG4 isotype-treated animals, anti-hCD79A treatment leads to a highly significant decrease in both IgM and IgD on the surface of splenic B cells. This is similar to the observations of Hardy et. al. using surrogate anti-mouse CD79B ([9], Fig 5B). This effect is different than that seen upon induction of B cell anergy, wherein cells express normal levels of IgD and decreased levels of IgM on their surface. Given the confirmation of binding and the initial cues from *in vivo* biologic activity, we wished to further characterize B cell receptor signaling in animals treated with anti-human CD79A.

To interrogate membrane-proximal BCR signaling events in anti-hCD79A-treated animals, we first assayed global BCR-induced tyrosine phosphorylation by western blot (Fig 3D). As before, 18 hours prior to the assay, cCD79A mice received 250 μg IP injections of either hIgG4 D265A anti-human CD79A or control hIgG4. Splenic B cells were harvested via CD43 negative cell selection and rested in serum free medium at 37°C for 1 hour before stimulation with either goat $F(ab')_2$ anti-mouse IgM or pervanadate. Whole B cell lysates were fractionated by SDS-PAGE and electrophoretic transfer to PVDF membranes. These were blotted with anti-phospho- tyrosine [4G10] and anti-actin. Unstimulated cells (0') serve to demonstrate basal tyrosine phosphorylation. Whereas actin blots control for equal protein loading, stimulation with the protein-tyrosine phosphatase inhibitor pervanadate controls for kinase activity and substrate availability (Fig 3D right). Most notably, global BCR-mediated tyrosine phosphorylation is impaired in B cells from anti-hCD79A-treated animals. The arrow-indicated band between the 70 and 95 kDa markers most likely represents spleen tyrosine kinase (Syk) and appears to be significantly diminished in the corresponding anti-hCD79A-treated lanes, at 1- and 10-minutes post BCR stimulation. To this end, identical sets of cell lysates were used to confirm Syk phosphorylation directly (Fig 3E). Having confirmed that BCR-induced Syk phosphorylation is significantly reduced in anti-hCD79A treated B cells, we next wanted to reconcile this signaling defect with decreased mIgM and mIgD expression. To do this we harvested spleens from cCD79A mice, treated as before, and stimulated RBC-lysed splenocytes with goat $F(ab')_2$ anti-mouse IgM for 5 minutes. Cells were immediately fixed before surface staining with anti-B220 and a non-stimulating, fluorescently-conjugated Fab anti-mouse Ig (H+L). This method of staining allowed us to gate on cells bearing equivalent levels of mBCR while analyzing Syk phosphorylation. Cells

Author Manuscript Author Manuscript Author Manuscript Author Manuscript

that had been fixed and surface stained were permeabilized and stained for intracellular phosphorylated Syk (Y525). As shown in figure 3F, when we normalized for mBCR surface expression, anti-hCD79A-treated cells showed decreased phosphorylation of Syk in response to IgM stimulation.

Considering the above observation, we next analyzed calcium mobilization as a function of BCR surface expression. As before, cCD79A animals received anti-hCD79A IP injection 18 hours prior to spleen excision. RBC-lysed splenocytes were stained with anti-B220 and Fab anti-mIg (H+L) while being loaded with the ratiometric calcium indicator, INDO. On a UV laser-equipped flow cytometer, indo emissions were collected for 30 seconds, to establish relative basal intracellular calcium concentrations, before stimulating cells with either 1 or 10 μg/mL rat anti-mouse IgM [B76] and acquiring data for an additional 150 seconds. Similar to Syk phosphorylation, when we analyze BCR-induced calcium mobilization by first gating on cells bearing equivalent mBCR, the suppressive effects of anti-hCD79A treatment remain (Fig 4A). Ionomycin stimulation induces calcium flux in anti-hCD79A-treated cells to the level of isotype control-treated cells (Fig 4B). BCR-mediated calcium mobilization is also suppressed in Ramos B cells after overnight culture with hIgG4 D265A anti-hCD79A (Fig 4C). Taken together, these observations imply that the inhibition of BCR signaling in anti-hCD79A-treated B cells is, at least partially, independent of the coincident reduction in mBCR and suggests that regulatory circuitry and/or receptor destabilization may be elicited by the treatment [34, 35] [36, 37].

Of particular interest in the study of anergic B cells, and their activity in health and disease, is the inhibitory phosphatase PTEN or Phosphatase and TENsin homolog [38]. PTEN is an inositol lipid phosphatase that opposes the activity of PI3 kinase and therefore regulates BCR signaling. PTEN can be observed at increased levels in anergic ($B_{ND}$) cells in humans and mice, and its dysregulation, i.e. reduction, is associated with autoimmune pathogenesis [39] [26] [38] [40]. Further, targeted overexpression of PTEN in mouse B cells causes refractory BCR signaling and inhibition of B cell immune responses *in vivo* [26]. For these reasons we assayed intracellular PTEN expression in B cells taken from animals injected with anti-hCD79A. Figure 4D demonstrates increased PTEN expression in cCD79A B cells 18 hours post injection. Importantly, the level of increase is consistent with those seen in human anergic B cells and in mouse models of anergy. In order to formally test PTEN's contribution to anti-CD79-induced anergy, we utilized a conditional and tissue specific mouse model of PTEN deletion, i.e. hCD20-$Cre^{TAM}$ X ROSA26-STOPflox-YFP X $PTEN^{flox/flox}$ (or $PTEN^{wt}$). These mice do not express human CD79 extracellular domains, which required that we use the surrogate anti-mouse CD79B antibody. Mice were first injected IP with 2 mg of tamoxifen on d0 to activate CRE and delete PTEN [26]. On d7, when intracellular PTEN becomes undetectable, mice were injected IP with 250 μg of either mouse IgG2a D265A anti-mouse CD79B or control mouse IgG2a anti-HEL. After 18 hours, we analyzed PTEN expression, antibody coating, and calcium mobilization in $B220^{+}YFP^{+}$ splenocytes. Figure 4E confirms PTEN knock-out was successful in both treated and control-treated animals. Anti-CD79-induced PTEN increase in wild-type animals can also be seen. Further, we demonstrated that B cells in anti-mCD79B-treated animals are coated with the therapeutic as shown by surface staining with an anti-mIgG2a. When these cells are subjected to BCR stimulation and calcium analysis, we see that the removal

Author Manuscript Author Manuscript Author Manuscript Author Manuscript

of PTEN leads to increased maximal intracellular calcium in B cells from anti-mCD79B-treated animals but not isotype control-treated animals. This noted loss of PTEN does accelerate response kinetics in isotype control-treated B cells (Fig 4F). These findings suggest that PTEN elevation plays a role in the reduced responsiveness of B cells exposed to anti-mCD79B, *in vivo*. Preliminary observations in SHP1 KO and SHIP-1 KO experiments showed no requirement for these molecules in anti- mCD79B modulation of BCR signaling (Wemlinger and Cambier, unpublished observations). These results lead us to believe that anti-CD79-induced desensitization of the BCR may involve multiple, partially redundant mechanisms in addition to receptor modulation. Moving forward, we wished to interrogate anti-hCD79A's effects on B cell immune responses.

### Anti-human CD79 treatment modulates primary B cell antibody responses to antigen and reduces antibody secretion by terminally differentiated plasmablasts and plasma cells.

The ability to inhibit a thymus-dependent (TD) antibody response to immunization with NP-conjugated ovalbumin was previously demonstrated in Hardy's anti-mouse CD79B experiments [9]. Herein we chose to first assess the impact of anti-human CD79 treatment on thymus-independent (TI) antibody responses, which rely on high valency BCR stimulation without T cell help. Antigens with highly repetitive BCR epitopes are capable of stimulating B cells to produce low affinity IgM antibodies that provide early protection from infection. To test the impact of anti-hCD79A treatment in this regard, cCD79A animals received either hIgG4 D265A anti-human CD79A, or control hIgG4, 24 hours before being immunized with $NP_{59}$-ficoll. Figure 5A shows a significant reduction (~80%) in the number of NP-specific $IgM^+$ antibody secreting cells (ASC) detectable 7 days post immunization in animals injected with anti-human CD79A. The development of high affinity IgG antibodies is a function of complex cellular interactions and processes that take place within germinal centers. These are specialized structures within secondary immune tissues that promote B cell proliferation, class switching, and affinity maturation of their B cell receptors [41]. Before confirming the findings involving anti-mouse CD79B, we looked at the effect of anti-hCD79A treatment on germinal center formation. To accomplish this, we treated cCD79A mice as before and then immunized with sheep red blood cells (SRBC) [23]. At 5 days post, splenic B cells from immunized mice were analyzed by flow cytometry for germinal center (GC) B cell markers, CD95/Fas and GL7. Figure 5B shows significant reduction (>50%) in both proportion and number of splenic B cells expressing these markers. These results provide at least a partial explanation for anti-CD79's ability to inhibit TD antibody responses. To confirm and translate the effects of anti-mouse CD79B on TD antibody responses, we immunized cCD79A mice, injected 24 hours prior with anti-hCD79A or control antibody, with NP-Ova in alum and enumerated NP-specific ASC 16 days later. Figure 5C shows a significant reduction (~60%) of $IgM^+$ anti-NP ASC found in the anti-hCD79A-injected mice. In addition, both total and high affinity $IgG^+$ anti-NP ASC are significantly reduced (>75%) in the same mice. These observations corroborate the activity of the surrogate anti-mouse CD79B and extend them to include suppressive effects on immune responses to immunization with TI antigens.

So far, we have focused on the effects of anti-CD79 treatment as a preventative measure. Pre-treatment with anti-CD79 strongly inhibits BCR signaling and primary B cell antibody

Author Manuscript Author Manuscript Author Manuscript Author Manuscript

responses. In other words, anti-CD79 is shown to act early in B cell activation by BCR stimulation or immunization. From a potentially therapeutic standpoint, it might be important to know the effects of anti-CD79 on terminally differentiated autoantibody secreting cells. The ability to suppress pathogenic autoantibody secretion would be beneficial in diseases such as SLE and would further differentiate anti-CD79 from anti-CD20, which does not target these cells (i.e. plasmablasts and plasma cells). As a pioneering step towards this possibility, we generated NP-specific ASC by immunizing cCD79A mice, as before, with NP-ova in alum and harvested spleens 16 days later. RBC-lysed splenocytes were then cultured overnight with either anti-hCD79A D265A, anti-mouse CD20 [18B12], or isotype control antibody (hIgG4 or mIgG2a). Following overnight incubation, cells were washed, counted and loaded onto NP-coated ELISPOT plates. The left panel of figure 5D shows a significant decrease in ASCs in overnight cultures containing anti-hCD79A, but not in cultures with anti-mCD20, as compared to control antibody cultures. It is important to note that no differences in splenocyte viability, i.e. trypan blue staining, were observed following overnight culture. As an additional experiment, we obtained PBMCs from subjects who received a tetanus booster (Tdap) 7–10 days prior to isolation. These PBMCs were cultured as before with either anti-hCD79A D265A, anti-hCD20 (Rituximab), or control hIgG4. Following overnight incubation, cells were washed and counted before being loaded onto tetanus-toxoid-coated ELISPOT plates. The right panel of figure 5D shows a similar decrease in TT-specific ASC when cells were cultured with Fc effector function-incompetent anti-hCD79A but not with anti-hCD20. These preliminary findings suggest that anti-CD79 may be capable of targeting and suppressing antibody secretion by ASCs. Importantly, suppression of antibody secretion was not induced by anti-CD20, suggesting a potentially distinct range of use of anti-CD79 therapy. Further experimentation is needed to understand the exact mechanism of ASC modulation by anti-CD79 and whether the treatment effects are preserved *in vivo*. Given these results we wished to look at anti-hCD79A treatment effects on autoantibody production.

To assess the potential impact of anti-hCD79A on development of autoimmunity, we next explored the *in vivo* prophylactic effects of anti-human CD79A in the pristane induction model of SLE [42]. cCD79A mice were pretreated on d0 with 250 μg IP of either hIgG4 isotype control antibody or human IgG4 anti-hCD79A D265A (Fig 5E). Mice then received a single 0.5 mL IP dose of pristane and were injected with antibody every 7 days thereafter. Normal mortality was observed in the first 30 days of the experiment, most likely due to pulmonary hemorrhage. There was no significant difference in survival rate between the groups and autoantibody was not detectable during this time. This suggests anti-hCD79A treatment does not modulate pristane-induced inflammatory processes operating early in the pristane model. Importantly, anti-hCD79A-treated mice failed to accumulate chromatin-specific IgG autoantibodies during the course of the experiment. We hypothesize that, in addition to preventing anti-chromatin autoantibody formation, extended prophylactic treatment with anti-hCD79A prevents the development of lupus-associated pathology in pristane-induced mice. Further experimentation is needed to measure anti-CD79's effects on autoantibody production to antigens other than chromatin as well as modulation of disease in fully therapeutic application.

Author Manuscript Author Manuscript Author Manuscript Author Manuscript

## Anti-human CD79 treatment prevents autoimmune disease development in experimental autoimmune encephalomyelitis

Early validation of the potential therapeutic efficacy of CD79 targeting was carried out by independent laboratories using surrogate anti-mouse CD79B antibodies in multiple disease models [8] [9] [10]. First described in the MRL/*lpr* model of systemic lupus erythematosus (SLE), anti-mouse CD79B prevented onset of spontaneous lupus-like disease in these mice, which was reportedly dependent on B cell depletion [8]. Importantly, treated mice accumulated far less chromatin-reactive IgG antibodies in their serum and displayed improved survival and lower mean skin scores. More recently, it has been found that targeting mouse CD79B prevents disease independent of its abilities to deplete B cells, rather acting by induction of reversible anergy [9]. In 2014, Hardy et. al. prevented development of severe arthritic disease in collagen-immunized mice. Importantly, these studies used mouse IgG2a anti-mouse CD79B antibodies that contained the D265A mutation, significantly reducing ADCC and CDC effector functions, thus preventing B cell depletion [43]. In contrast, when formulated in this fashion, anti-CD20 no longer induced B cell depletion and did not protect mice from developing anti-collagen autoantibodies and consequent joint inflammation. The effects of non-depleting anti-mCD79B on B cells were maintained as long as ~20% of BCR were engaged by antibody, as B cells recover their signaling ability after anti-mCD79B levels decay. Use of non-depleting therapy has potential to mitigate safety concerns associated with long-term B cell depletion. This mode of protection from collagen-induced arthritis was confirmed by Brühl and company the following year [10]. Their findings suggest that the tolerizing effects of anti-mCD79B extend beyond the BCR, potentially modulating signals emanating from CD40 and CD180. Apart from inducing anergy in B cells, other investigators are exploring CD79 targeting with CAR-T cells and drug-antibody conjugates for treatment of B cell malignancies [44, 45].

We sought additional evidence of clinical utility of anti-hCD79A antibodies using the B cell dependent EAE model of multiple sclerosis [46] [47]. Male and female $cCD79A^{+/+}cCD79B^{+/-}$ mice were immunized IP with 50 μg recombinant human myelin oligodendrocyte glycoprotein ($hMOG_{1–125}$) in 200 μg complete Freund's adjuvant (CFA) on day 0. Mice also received IP injections containing 200 ng pertussis toxin in PBS on d0 and d2. Mice were given weekly IP injections of antibody at 20 mg/kg of body weight, beginning on d-3 and continuing for the duration of the experiment. Antibody treatment arms consisted of aglycosyl-mIgG1 anti-hCD79A (anergizing), mIgG2a anti-hCD79A (depleting), and both aglycosyl-mIgG1 and mIgG2a anti-HEL isotype controls. Figure 6A demonstrates that the anti-human CD79A formulation that is non-depleting is, nonetheless, efficacious. In this experiment aglycosylated mIgG1 anti-human CD79A antibody was used to prevent ADCC and CDC leading to B cell killing, thus isolating anergizing function, while anti-human CD79 antibody in IgG2a format was used for B cell depletion. Depleting and anergizing anti-hCD79A antibodies reduced EAE disease severity similarly, to a degree equivalent to depleting anti-CD20 antibodies [48] [49]. Incidence of EAE was drastically reduced for the anergy and depletion groups compared to the isotype groups in this study (anergy 56.3%; depletion 58.8%; pooled isotype 94.7%) (Fig 6B). A significant delay in disease onset was also observed in the anti-hCD79A-treatment groups (median day of onset: anergy 14; depletion 13.5; pooled isotype 12). Surprisingly, mice treated with

Author Manuscript Author Manuscript Author Manuscript Author Manuscript

anergizing anti-hCD79A tended to be protected from weight loss over the duration of the experiment (Fig 6C). Importantly, B cell depletion was seen in EAE mice receiving wild-type mIgG2a anti-hCD79A while B cells were not significantly depleted in mice receiving the aglycosylated mouse IgG1 anti-hCD79A (Fig 6D, left). Both anti-hCD79A antibody treatments caused reduced expression of surface IgD, a unique property of anti-CD79 induced B cell anergy as it is not a characteristic of anergic B cells (Fig 6D, right). No significant differences were observed in other immune cells (i.e. CD4, CD8, Myeloid) in response to either anti-hCD79A treatments (Fig 6E). Figure 6F demonstrates highly significant reduction in relative serum concentrations of anti-MOG IgG in mice receiving either anti-hCD79A treatments. Isotype treatment groups display rapid onset of anti-MOG antibody production while minimal levels are found in the anti-hCD79A treatment groups throughout the duration of the experiment. At the peak of disease (d15) significantly decreased anti-MOG IgG in the anergized mice suggests inhibited B cell activation leading up to the peak of exacerbation in EAE-associated paralysis. Significantly reduced serum pNfH, a marker of neurodegeneration, at the peak of disease is also seen in mice treated with anergizing anti-hCD79A (Fig 6G).

In conclusion, we have confirmed the ability of anti-human CD79A antibodies to prevent autoimmune disease development in humanized cCD79 mice. Paramount in these experiments is demonstration that the ability of anti-human CD79A antibody to prevent development of autoimmunity is independent of its ability to deplete B cells. In the pristane model, anti-hCD79A was rendered Fc effector-compromised by virtue of the D265A mutation. Similar Fc mutational approaches are utilized in therapeutic antibodies currently being administered to patients [50]. Blocking the development of anti-chromatin, and potentially other autoantibodies induced by pristane, suggests prevention of outright disease. In the EAE model of multiple sclerosis, anti-human CD79A antibodies also prevented disease in the absence of B cell depletion. Non-depleting therapies that target B cells represent a potentially safer alternative to CD20-mediated B cell depletion.

## Discussion

Here we describe the generation and application of a humanized mouse platform for preclinical validation of candidate anti-human CD79 therapeutic antibodies. This approach is advantageous in situations in which the therapeutic target dictates need for an in-depth understanding of immunological impact of the intervention that is not achievable in non-human primates. In this case, knock-in mice were created that express, in context, the extracellular domains of either or both human CD79A and B. These mice were used to study the functional interchangeability of human and mouse CD79 extracellular domains, and the activity of a humanized IgG4 D265A anti-human CD79A monoclonal antibody hypothesized to suppress immune responses, including autoimmune responses, by inducing an anergic-like state without significant B cell depletion.

CD79 heterodimers associate non-covalently with immunoglobulins and are required for membrane expression of the B cell receptor; without CD79 expression, B cell development is arrested at the pro- to pre-B cell transition [1]. In addition to its roles in B cell development, CD79 ITAMs are responsible for initiating intracellular signaling cascades

Author Manuscript Author Manuscript Author Manuscript Author Manuscript

subsequent to aggregation of the BCR [51]. These signals ultimately drive B cell activation, proliferation, and differentiation in immune responses [52]. Human CD79 heterodimers are similar structurally to those found in mice. Both consist of CD79A-CD79B disulfide-linked heterodimers which associate with surface immunoglobulin in B cell plasma membranes. CD79A and CD79B each have a single extracellular immunoglobulin-like domain, a single pass transmembrane domain, and cytoplasmic signaling domains. CD79 sequence homology between mouse and human is lowest in the extracellular Ig-like domains, suggesting a potential lack of cross-reactivity between anti-human and anti-mouse CD79 antibodies. Highest conservation between these species can be found in the transmembrane and cytoplasmic domains. The TM domain of CD79A is 100% conserved in mice and humans. This is also true of the membrane spanning domains of membrane-bound IgM, which is believed to contain the site of interaction with CD79A [53]. To this end, surface expression of IgM in mouse B cells is achievable with expression of the human CD79A encoding gene, *mb-1* [54]. Further, humans expressing mutated CD79A, which resulted in a loss of the CD79A TM domain, lack peripheral B cells and are agammaglobulinemic [55] [56]. Thus, it was predicted that expression of our chimeric CD79, in which only the extracellular domain sequences are human, would not disrupt BCR assembly in mice. Data presented here confirms this prediction. Due to the low sequence homology between mouse and human CD79 extracellular Ig-like domains, we hypothesize that interactions between the Ig-domains of CD79 and membrane immunoglobulin are much less important than those within the transmembrane domains of each.

Our findings lead to a number of conclusions. Because CD79 plays a critical role in B cell development and function, and because human CD79 could disrupt these functions, we characterized the cCD79 knock-in mouse lines in comparison to wild type C57BL/6 mice. Results indicate that human and mouse CD79 extracellular domains are interchangeable in all regards. Our analyses show B cell developmental populations within the bone marrow and the spleen to be within normal ranges. Similarly, B cell activation and differentiation in the periphery is normal. BCR signaling and B cell immune responses were found to be unaffected by CD79 extracellular domain replacement. Although cCD79 B cells behave in a nearly identical fashion as wild type B cells expressing mouse CD79, we addressed several interesting findings that came to light in our studies. First, the observed relative mass of our cCD79B molecule is closer to the known mass of mouse CD79B (Fig 1E, middle membrane). Specifically, mouse CD79B migrates at 37kDa while fully human CD79B migrates at 34kDa [57] [58]. Our chimeric human-mouse CD79B migrates at ~35kDa suggesting that the differences may be associated with the cellular context and/or glycosylation. Another puzzling observation is the apparent preference of cCD79A for pairing with the endogenous mouse CD79B molecule on the surface of B cells in $cCD79A^{+/+}B^{+/-}$ mice. However, there are no discrepancies in IgM nor IgD expression levels between cCD79A mice expressing either no, one, or both copies of cCD79B. In addition, no discrepancies in B cell development nor BCR function were observed in singly homozygous, e.g. cCD79A and cCD79B, mice suggesting that the staining seen in Fig 1D and Fig 1G is due to the relative affinities of the monoclonal antibodies.

We further report that in WT and knock in mice, respectively, anti-mouse and anti-human CD79 antibodies have similar inhibitory effects on BCR signaling and on immune

Author Manuscript Author Manuscript Author Manuscript Author Manuscript

responses. Chronic stimulation of the BCR by autoantigen in the absence of secondary signals induces a form of peripheral B cell tolerance known as anergy [59] [60] [61] [62]. Chronic engagement of the BCR via anti-CD79 antibodies elicits a signaling phenotype similarly observed in anergic B cells [63]. Hardy's anti-mouse CD79B experiments demonstrated decreased IgM and IgD expression in response to treatment *in vivo* [9]. BCR-mediated calcium signaling was also observed to be suppressed in these B cells. However, reduced calcium signaling was not shown to be independent of decreased membrane BCR. Herein, we have demonstrated that the humanized IgG4 D265A anti-human CD79A clinical candidate induces inhibition of BCR-mediated Syk phosphorylation and calcium mobilization that is independent of changes in IgM and IgD surface expression. In comparison to anergic B cells, anti-CD79 treatment induces down modulation of both IgM- and IgD-containing B cell antigen receptors. The ability to affect mIgD expression, a unique trait of anti-CD79 treatment, could be due to the expression pattern of IgM and IgD on peripheral B cells that are likely the primary target of the therapeutic, e.g. mature naïve B cells in peripheral blood and spleen. Developing autoreactive, and potentially anergic, B cells in the bone marrow encounter autoantigen upon expression of their IgM pre-BCR, prior to expression of IgD. This difference suggests that mIgD on anergic B cells may not bind antigen with the same efficiency as mIgM. This would be consisted with the greater length IgM heavy chains (5 Ig domains) relative to IgD heavy chains (3 Ig domains). In addition, we confirm that ionomycin-induced calcium mobilization is unaffected by prior treatment with anti-CD79. These observations suggest that similar to anergic B cells, anti-CD79 treatment targets signaling events proximal to the BCR and may also rely on non-durable mechanisms.

In addition to effects on BCR signaling, *in vivo* treatment with anti-human CD79 induces increased intracellular expression of the regulatory phosphatase, PTEN. PTEN expression in cCD79A B cells is increased by anti-human CD79A treatment to levels consistent with those observed in human anergic $B_{ND}$ cells [38]. However, targeted genetic ablation of PTEN in mice resulted in modest increases in BCR-mediated calcium flux in cells treated with anti-CD79A. We hypothesize that PTEN may play a partial role in the mechanism; suppression of signaling may involve multiple, partially redundant mechanisms including mBCR modulation, regulatory signaling, and potential disassociation of the BCR signaling complex. Another possibility includes preferential monophosphorylation of CD79 ITAMs in cells treated with anti-CD79 [35]. The known consequence of ITAM monophosphorylation is activation of Lyn-mediated inhibitory signaling pathways, but not Syk [64]. Considering what is known about PTEN-mediated regulation of phosphoinositide 3-kinase (PI3K) signaling, anti-CD79 treatment may also affect signaling by other activating receptors, e.g. CD40, toll-like receptors, and cytokine/chemokine receptors [65]. Data presented by Brühl et. al., suggests inhibition of CD40 and CD180 signaling by treatment with anti-mouse CD79 [10]. Further, because signaling by the receptor for B cell activating factor (BAFFR) has been shown to involve subunits of the BCR as adaptor molecules [66], anti-CD79 treatment may also modulate BAFF signaling. Additional experimentation is needed to fully define the molecular mechanisms operative in anti-CD79-induced B cell anergy.

We confirm and extend anti-CD79 effects on B cell immune responses to include those induced by immunization with TI and TD antigens. Not surprisingly, pre-treatment with

Author Manuscript Author Manuscript Author Manuscript Author Manuscript

anti-CD79 resulted in significantly diminished recovery of $CD95^+GL7^+$ germinal center B cells in response to immunization with SRBCs. Perhaps more interesting from a therapeutic standpoint is the potential for anti-CD79 treatment to effect antibody secretion by terminally differentiated B cells. There is currently a need for therapies targeting secreting cells in diseases characterized by pathogenic autoantibody. Precedent for this mode of inhibition was demonstrated in an IgM-secreting hybridoma specific for the hapten fluorescein [67]. In 1980, Boyd and Schrader showed that antigen binding to the surface of these cells induced inhibition of protein synthesis and antibody secretion. More recently it has been demonstrated that $IgM^+$ and $IgA^+$ human plasma cells (PC) express surface BCR and that high doses of BCR-crosslinking antibody leads to significantly impaired recovery of ASC [68]. Importantly, it was shown that all human PCs, i.e. $IgM^+$, $IgA^+$, and $IgG^+$, stained positive for the intracellular portions of CD79 ($Ig_\alpha$ and $Ig_\beta$) suggesting that surface expression of CD79 may be maintained irrespective of surface immunoglobulin. Here we show that *in vitro* anti-CD79 treatment results in significantly reduced recovery of antigen specific ASC. Importantly, antibodies targeting CD20 did not induce this effect. Based on the level of inhibition, we hypothesize that at least some ASC express CD79 and that treatment with anti-CD79 negatively affects antibody secretion. At this time we are unsure if anti-CD79 treatment affects short lived plasmablasts, long lived plasma cells, or both. It is also unclear whether treatment suppresses antibody secretion and/or induces cell death. Further experimentation is needed in order to better understand this phenomenon and whether or not treatment effects are maintained *in vivo*. We are excited about the possibility that CD79 targeting may be successful at both preventing autoimmune B cell responses and at disrupting those responses that are already underway.

Most promising from the preclinical testing perspective were anti-hCD79A's effects on pristane induced autoantibody production and EAE disease development. In pristane-injected mice receiving anti-hCD79A, little to no anti-chromatin autoantibody is detected after 2 months, unlike isotype control mice. Currently, our research efforts include validating fully therapeutic application of anti-hCD79A in this model. We anticipate that this approach will also help to clarify anti-CD79's therapeutic effect on terminally differentiated ASCs specific for lupus-associated autoantigens. In a preventative treatment of EAE, anti-human CD79A greatly reduced disease severity and incidence and lead to near complete recovery. The magnitude of this effect was equal to or greater than that induced by B cell depletion using either anti-CD20 or fully competent anti-hCD79A. Similar to previous reports using effector function-compromised anti-mouse CD79B, disease modulation by anti-human CD79A was achieved without significant B cell depletion, which is the main mechanism of action exploited by current B cell targeting clinical therapies [69]. At takedown, 30 days post immunization with $hMOG_{1–125}$, we observe a non-significant reduction in splenic B cells in mice receiving anergizing anti-hCD79A. However, there is a downward trend that is reminiscent of B cell counts in the peripheral blood (PB) of Hardy's mice treated with an effector function-compromised anti-mouse CD79B ([9], Fig 4B). By 4 weeks post injection, PB B cell numbers matched those of isotype control animals. Although there was a transient reduction in PB B cells for ~3 weeks following a single injection, B cells in mice treated with mutated (D265A) anti-mCD79B did not label with BrdU within this timeframe ([9], Fig 7). It was concluded that treatment with the surrogate, non-depleting anti-mCD79B

Author Manuscript Author Manuscript Author Manuscript Author Manuscript

induced a transient relocation of PB B cells. These observations support the potential impact of anti-CD79 on other receptors expressed by B cells, e.g. chemokine receptors. At the peak of EAE disease (d15), mice in the anergizing treatment arm were observed to have significantly reduced serum concentrations of phosphorylated neurofilament heavy chain (pNfH), a marker of neurodegeneration [70]. This measure is a correlate of reduced paralysis and reduced relative serum anti-MOG autoantibodies. Taken together, these observations suggest that anergizing anti-hCD79A treatment inhibits activation of autoreactive anti-MOG B cells, which prevents the development of severe EAE. We hypothesize that inhibiting B cells in this model modulates disease in part by down-regulating B cell antigen presentation to CD4 T cells. It has previously been shown that expansion of antigen-specific (MOG) B cells, in mice expressing MHC class II on B cells alone, and therefore the sole antigen presenting cell, drives EAE associated neuroinflammation [71]. Further experimentation is needed to directly assess the impact of anergizing anti-CD79A treatment on B cell antigen presentation. We also wish to test this treatment in fully therapeutic mode, administering antibody at the peak of clinical disease.

We conclude that anti-CD79 functions by inducing transient anergy in autoreactive B cells. Not only does this predict success of CD79 targeted therapies, but it also addresses potential safety concerns associated with depleting therapies [18]. Historically, anti-CD20-mediated B cell depletion leads to a significant reduction of B cells in mouse peripheral blood for > 40 days post-injection ([9], Fig4A). Preliminary experiments demonstrate that B cell functionality is fully restored at 35 days post injection with Fc effector function-compromised anti-hCD79 (Wemlinger and Cambier, unpublished observations). Confirmation of these findings would support reversibility of anti-hCD79 treatment effects, offering an additional potential advantage over current B cell depleting therapies. Finally, the potential to inhibit autoantibody secretion by terminally differentiated plasmablasts and/or plasma cells could further differentiate CD79 targeting from CD20, which is not expressed on these cells.

Because anti-CD79 therapy relies on modulation of BCR signaling and B cell immune responses, it is important to define the mechanism of action in mouse B cells. The advantages of a murine preclinical model revolve around the more advanced state of our knowledge of and ability to manipulate the mouse immune system, as well as the prohibitive expense of preclinical studies in monkeys. Further, non-cross reactivity of anti-human CD79 antibodies in cynomolgus monkeys presents a significant obstacle to preclinical validation of candidate therapeutic monoclonals. If necessary, a surrogate anti-cyno CD79 antibody can be used to assess toxicology in non-human primates [45, 72]. We believe that our humanized mouse line represents an ideal preclinical model.

## Supplementary Material

Refer to Web version on PubMed Central for supplementary material.

## Acknowledgements

The authors would like to thank the following groups: The Mouse Genetics Core Facility at National Jewish Health (Denver, CO) for producing singly heterozygous cCD79 A and cCD79B mice; The Office of Laboratory Animal

Author Manuscript Author Manuscript Author Manuscript Author Manuscript

Resources at the University of Colorado Anschutz Medical Campus (Aurora, CO) for housing and caring for our mouse colony; The CU | AMC ImmunoMicro Flow Cytometry Shared Resource for providing and maintaining flow cytometry equipment, RRID:SCR_021321; Panorama Research (Sunnyvale, CA) for humanization and affinity maturation of anti-human CD79 antibodies; The Raul Torres Lab at CU Anschutz for providing positive control sera from diseased SLE1.2.3 mice; The Lawrence Wysocki Lab at National Jewish Health for providing purified calf chromatin; Gisela Vaitaitis from the David Wagner lab at CU Anschutz for assisting with EAE induction; G. Campbell Kaynor and Kathryn Pellerin with the Multiple Sclerosis and Neurorepair Research Unit at Biogen for phospho-NF-H assays and anti-MOG ELISAs, respectively; and Mia Rushe and Joseph Amatucci with the Biologics Drug Discovery Unit at Biogen for preparation of the dosing solutions.

Grant support was provided by the following funding sources: R01 AI124487 (PI Cambier); R44 AI120433 (PI Larrick); DP3 DK110845 (PIs Michaels and Cambier)

## References

1. Pelanda R, Braun U, Hobeika E, Nussenzweig MC, and Reth M: B Cell Progenitors Are Arrested in Maturation but Have Intact VDJ Recombination in the Absence of Ig-α and Ig-β. The Journal of Immunology 2002, 169(2):865. [PubMed: 12097390]
2. Cambier JC: Antigen and Fc receptor signaling. The awesome power of the immunoreceptor tyrosine-based activation motif (ITAM). J Immunol 1995, 155(7):3281–3285. [PubMed: 7561018]
3. Reth M: Antigen receptor tail clue. Nature 1989, 338(6214):383–384. [PubMed: 2927501]
4. Van Noesel CJ, Brouns GS, Van Schijndel GM, Bende RJ, Mason DY, Borst J, and Van Lier RA: Comparison of human B cell antigen receptor complexes: membrane-expressed forms of immunoglobulin (Ig)M, IgD, and IgG are associated with structurally related heterodimers. J Exp Med 1992, 175(6):1511–1519. [PubMed: 1375264]
5. Flaswinkel H, and Reth M: Dual role of the tyrosine activation motif of the Ig-alpha protein during signal transduction via the B cell antigen receptor. The EMBO Journal 1994, 13(1):83–89. [PubMed: 8306975]
6. Sakaguchi N, Kashiwamura S, Kimoto M, Thalmann P, and Melchers F: B lymphocyte lineage-restricted expression of mb-1, a gene with CD3-like structural properties. Embo j 1988, 7(11):3457–3464. [PubMed: 2463161]
7. Hermanson GG, Eisenberg D, Kincade PW, and Wall R: B29: a member of the immunoglobulin gene superfamily exclusively expressed on beta-lineage cells. Proc Natl Acad Sci U S A 1988, 85(18):6890–6894. [PubMed: 3137575]
8. Li Y, Chen F, Putt M, Koo YK, Madaio M, Cambier JC, Cohen PL, and Eisenberg RA: B cell depletion with anti-CD79 mAbs ameliorates autoimmune disease in MRL/lpr mice. J Immunol 2008, 181(5):2961–2972. [PubMed: 18713966]
9. Hardy IR, Anceriz N, Rousseau F, Seefeldt MB, Hatterer E, Irla M, Buatois V, Chatel LE, Getahun A, Fletcher A et al. : Anti-CD79 antibody induces B cell anergy that protects against autoimmunity. J Immunol 2014, 192(4):1641–1650. [PubMed: 24442438]
10. Brühl H, Cihak J, Talke Y, Rodriguez Gomez M, Hermann F, Goebel N, Renner K, Plachý J, Stangassinger M, Aschermann S et al. : B-cell inhibition by cross-linking CD79b is superior to B-cell depletion with anti-CD20 antibodies in treating murine collagen-induced arthritis. Eur J Immunol 2015, 45(3):705–715. [PubMed: 25471597]
11. Hauser SL, Waubant E, Arnold DL, Vollmer T, Antel J, Fox RJ, Bar-Or A, Panzara M, Sarkar N, Agarwal S et al. : B-cell depletion with rituximab in relapsing-remitting multiple sclerosis. N Engl J Med 2008, 358(7):676–688. [PubMed: 18272891]
12. Florou D, Katsara M, Feehan J, Dardiotis E, and Apostolopoulos V: Anti-CD20 Agents for Multiple Sclerosis: Spotlight on Ocrelizumab and Ofatumumab. Brain Sci 2020, 10(10).
13. Herold KC, Pescovitz MD, McGee P, Krause-Steinrauf H, Spain LM, Bourcier K, Asare A, Liu Z, Lachin JM, and Dosch HM: Increased T cell proliferative responses to islet antigens identify clinical responders to anti-CD20 monoclonal antibody (rituximab) therapy in type 1 diabetes. J Immunol 2011, 187(4):1998–2005. [PubMed: 21775681]
14. Korhonen R, and Moilanen E: Anti-CD20 antibody rituximab in the treatment of rheumatoid arthritis. Basic Clin Pharmacol Toxicol 2010, 106(1):13–21. [PubMed: 19686542]

Author Manuscript Author Manuscript Author Manuscript Author Manuscript

15. Shah K, Cragg M, Leandro M, and Reddy V: Anti-CD20 monoclonal antibodies in Systemic Lupus Erythematosus. Biologicals 2020.
16. Tahara M, Oeda T, Okada K, Kiriyama T, Ochi K, Maruyama H, Fukaura H, Nomura K, Shimizu Y, Mori M et al. : Safety and efficacy of rituximab in neuromyelitis optica spectrum disorders (RIN-1 study): a multicentre, randomised, double-blind, placebo-controlled trial. Lancet Neurol 2020, 19(4):298–306. [PubMed: 32199095]
17. Du FH, Mills EA, and Mao-Draayer Y: Next-generation anti-CD20 monoclonal antibodies in autoimmune disease treatment. Auto Immun Highlights 2017, 8(1):12. [PubMed: 29143151]
18. Luna G, Alping P, Burman J, Fink K, Fogdell-Hahn A, Gunnarsson M, Hillert J, Langer-Gould A, Lycke J, Nilsson P et al. : Infection Risks Among Patients With Multiple Sclerosis Treated With Fingolimod, Natalizumab, Rituximab, and Injectable Therapies. JAMA Neurology 2020, 77(2):184–191. [PubMed: 31589278]
19. Pettitt SJ, Liang Q, Rairdan XY, Moran JL, Prosser HM, Beier DR, Lloyd KC, Bradley A, and Skarnes WC: Agouti C57BL/6N embryonic stem cells for mouse genetic resources. Nat Methods 2009, 6(7):493–495. [PubMed: 19525957]
20. Valenzuela DM, Murphy AJ, Frendewey D, Gale NW, Economides AN, Auerbach W, Poueymirou WT, Adams NC, Rojas J, Yasenchak J et al. : High-throughput engineering of the mouse genome coupled with high-resolution expression analysis. Nat Biotechnol 2003, 21(6):652–659. [PubMed: 12730667]
21. Larrick J, Yu B, Mendelsohn A, and Cambier J: Anti-CD79 Antibodies and Their Uses. In. USA: Nepenthe Bioscience LLC; 2020.
22. Zhang C: Hybridoma technology for the generation of monoclonal antibodies. Methods Mol Biol 2012, 901:117–135. [PubMed: 22723097]
23. McAllister EJ, Apgar JR, Leung CR, Rickert RC, and Jellusova J: New Methods To Analyze B Cell Immune Responses to Thymus-Dependent Antigen Sheep Red Blood Cells. J Immunol 2017, 199(8):2998–3003. [PubMed: 28916524]
24. Smith MJ, Packard TA, O'Neill SK, Hinman RM, Rihanek M, Gottlieb PA, and Cambier JC: Detection and Enrichment of Rare Antigen-specific B Cells for Analysis of Phenotype and Function. JoVE 2017(120):e55382.
25. Racke MK: Experimental autoimmune encephalomyelitis (EAE). Curr Protoc Neurosci 2001, Chapter 9:Unit9.7.
26. Getahun A, Wemlinger SM, Rudra P, Santiago ML, Van Dyk LF, and Cambier JC: Impaired B cell function during viral infections due to PTEN-mediated inhibition of the PI3K pathway. J Exp Med 2017, 214(4):931–941. [PubMed: 28341640]
27. Radaev S, Zou Z, Tolar P, Nguyen K, Nguyen A, Krueger PD, Stutzman N, Pierce S, and Sun PD: Structural and functional studies of Igalphabeta and its assembly with the B cell antigen receptor. Structure 2010, 18(8):934–943. [PubMed: 20696394]
28. Lam KP, Kühn R, and Rajewsky K: In vivo ablation of surface immunoglobulin on mature B cells by inducible gene targeting results in rapid cell death. Cell 1997, 90(6):1073–1083. [PubMed: 9323135]
29. Meffre E, and Nussenzweig MC: Deletion of immunoglobulin beta in developing B cells leads to cell death. Proceedings of the National Academy of Sciences of the United States of America 2002, 99(17):11334–11339. [PubMed: 12165571]
30. Kraus M, Alimzhanov MB, Rajewsky N, and Rajewsky K: Survival of resting mature B lymphocytes depends on BCR signaling via the Igalpha/beta heterodimer. Cell 2004, 117(6):787–800. [PubMed: 15186779]
31. Dal Porto JM, Gauld SB, Merrell KT, Mills D, Pugh-Bernard AE, and Cambier J: B cell antigen receptor signaling 101. Mol Immunol 2004, 41(6–7):599–613. [PubMed: 15219998]
32. Scharenberg AM, Humphries LA, and Rawlings DJ: Calcium signalling and cell-fate choice in B cells. Nat Rev Immunol 2007, 7(10):778–789. [PubMed: 17853903]
33. Nutt SL, Hodgkin PD, Tarlinton DM, and Corcoran LM: The generation of antibody-secreting plasma cells. Nature Reviews Immunology 2015, 15(3):160–171.

Author Manuscript Author Manuscript Author Manuscript Author Manuscript


34. Getahun A, Beavers NA, Larson SR, Shlomchik MJ, and Cambier JC: Continuous inhibitory signaling by both SHP-1 and SHIP-1 pathways is required to maintain unresponsiveness of anergic B cells. J Exp Med 2016, 213(5):751–769. [PubMed: 27114609]
35. O'Neill SK, Getahun A, Gauld SB, Merrell KT, Tamir I, Smith MJ, Dal Porto JM, Li QZ, and Cambier JC: Monophosphorylation of CD79a and CD79b ITAM motifs initiates a SHIP-1 phosphatase-mediated inhibitory signaling cascade required for B cell anergy. Immunity 2011, 35(5):746–756. [PubMed: 22078222]
36. Vilen BJ, Famiglietti SJ, Carbone AM, Kay BK, and Cambier JC: B cell antigen receptor desensitization: disruption of receptor coupling to tyrosine kinase activation. The Journal of Immunology 1997, 159(1):231. [PubMed: 9200459]
37. Vilen BJ, Nakamura T, and Cambier JC: Antigen-stimulated dissociation of BCR mIg from Ig-alpha/Ig-beta: implications for receptor desensitization. Immunity 1999, 10(2):239–248. [PubMed: 10072076]
38. Smith MJ, Ford BR, Rihanek M, Coleman BM, Getahun A, Sarapura VD, Gottlieb PA, and Cambier JC: Elevated PTEN expression maintains anergy in human B cells and reveals unexpectedly high repertoire autoreactivity. JCI Insight 2019, 4(3):e123384.
39. Browne CD, Del Nagro CJ, Cato MH, Dengler HS, and Rickert RC: Suppression of phosphatidylinositol 3,4,5-trisphosphate production is a key determinant of B cell anergy. Immunity 2009, 31(5):749–760. [PubMed: 19896393]
40. Wu XN, Ye YX, Niu JW, Li Y, Li X, You X, Chen H, Zhao LD, Zeng XF, Zhang FC et al. : Defective PTEN regulation contributes to B cell hyperresponsiveness in systemic lupus erythematosus. Sci Transl Med 2014, 6(246):246ra299.
41. Victora GD, and Nussenzweig MC: Germinal centers. Annu Rev Immunol 2012, 30:429–457. [PubMed: 22224772]
42. Freitas EC, de Oliveira MS, and Monticielo OA: Pristane-induced lupus: considerations on this experimental model. Clin Rheumatol 2017, 36(11):2403–2414. [PubMed: 28879482]
43. Baudino L, Shinohara Y, Nimmerjahn F, Furukawa J, Nakata M, Martínez-Soria E, Petry F, Ravetch JV, Nishimura S, and Izui S: Crucial role of aspartic acid at position 265 in the CH2 domain for murine IgG2a and IgG2b Fc-associated effector functions. J Immunol 2008, 181(9):6664–6669. [PubMed: 18941257]
44. Zhang L, French RR, Chan HT, O'Keefe TL, Cragg MS, Power MJ, and Glennie MJ: The development of anti-CD79 monoclonal antibodies for treatment of B-cell neoplastic disease. Ther Immunol 1995, 2(4):191–202. [PubMed: 9358611]
45. Li D, Lee D, Dere RC, Zheng B, Yu SF, Fuh FK, Kozak KR, Chung S, Bumbaca Yadav D, Nazzal D et al. : Evaluation and use of an anti-cynomolgus monkey CD79b surrogate antibody-drug conjugate to enable clinical development of polatuzumab vedotin. Br J Pharmacol 2019, 176(19):3805–3818. [PubMed: 31270798]
46. Oliver AR, Lyon GM, and Ruddle NH: Rat and human myelin oligodendrocyte glycoproteins induce experimental autoimmune encephalomyelitis by different mechanisms in C57BL/6 mice. J Immunol 2003, 171(1):462–468. [PubMed: 12817031]
47. Marta CB, Oliver AR, Sweet RA, Pfeiffer SE, and Ruddle NH: Pathogenic myelin oligodendrocyte glycoprotein antibodies recognize glycosylated epitopes and perturb oligodendrocyte physiology. Proceedings of the National Academy of Sciences of the United States of America 2005, 102(39):13992–13997. [PubMed: 16172404]
48. Monson NL, Cravens P, Hussain R, Harp CT, Cummings M, de Pilar Martin M, Ben LH, Do J, Lyons JA, Lovette-Racke A et al. : Rituximab therapy reduces organ-specific T cell responses and ameliorates experimental autoimmune encephalomyelitis. PLoS One 2011, 6(2):e17103-e17103.
49. Weber MS, Prod'homme T, Patarroyo JC, Molnarfi N, Karnezis T, Lehmann-Horn K, Danilenko DM, Eastham-Anderson J, Slavin AJ, Linington C et al. : B-cell activation influences T-cell polarization and outcome of anti-CD20 B-cell depletion in central nervous system autoimmunity. Ann Neurol 2010, 68(3):369–383. [PubMed: 20641064]
50. Kang TH, and Jung ST: Boosting therapeutic potency of antibodies by taming Fc domain functions. Experimental & Molecular Medicine 2019, 51(11):1–9.

Author Manuscript Author Manuscript Author Manuscript Author Manuscript


51. Johnson SA, Pleiman CM, Pao L, Schneringer J, Hippen K, and Cambier JC: Phosphorylated immunoreceptor signaling motifs (ITAMs) exhibit unique abilities to bind and activate Lyn and Syk tyrosine kinases. J Immunol 1995, 155(10):4596–4603. [PubMed: 7594458]
52. Packard TA, and Cambier JC: B lymphocyte antigen receptor signaling: initiation, amplification, and regulation. F1000Prime Rep 2013, 5:40–40. [PubMed: 24167721]
53. Reth M, Hombach J, Wienands J, Campbell KS, Chien N, Justement LB, and Cambier JC: The B-cell antigen receptor complex. Immunology Today 1991, 12(6):196–201. [PubMed: 1878135]
54. Hombach J, Tsubata T, Leclercq L, Stappert H, and Reth M: Molecular components of the B-cell antigen receptor complex of the IgM class. Nature 1990, 343(6260):760–762. [PubMed: 2304550]
55. Minegishi Y, Coustan-Smith E, Rapalus L, Ersoy F, Campana D, and Conley ME: Mutations in Igalpha (CD79a) result in a complete block in B-cell development. J Clin Invest 1999, 104(8):1115–1121. [PubMed: 10525050]
56. Wang Y, Kanegane H, Sanal O, Tezcan I, Ersoy F, Futatani T, and Miyawaki T: Novel Igα (CD79a) gene mutation in a Turkish patient with B cell-deficient agammaglobulinemia. American Journal of Medical Genetics 2002, 108(4):333–336. [PubMed: 11920841]
57. Friedrich RJ, Campbell KS, and Cambier JC: The gamma subunit of the B cell antigen-receptor complex is a C-terminally truncated product of the B29 gene. J Immunol 1993, 150(7):2814–2822. [PubMed: 8454858]
58. Clark MR, Friedrich RJ, Campbell KS, and Cambier JC: Human pre-B and B cell membrane mu-chains are noncovalently associated with a disulfide-linked complex containing a product of the B29 gene. J Immunol 1992, 149(9):2857–2863. [PubMed: 1401917]
59. Cyster JG, Hartley SB, and Goodnow CC: Competition for follicular niches excludes self-reactive cells from the recirculating B-cell repertoire. Nature 1994, 371(6496):389–395. [PubMed: 7522305]
60. Cooke MP, Heath AW, Shokat KM, Zeng Y, Finkelman FD, Linsley PS, Howard M, and Goodnow CC: Immunoglobulin signal transduction guides the specificity of B cell-T cell interactions and is blocked in tolerant self-reactive B cells. J Exp Med 1994, 179(2):425–438. [PubMed: 8294858]
61. Eris JM, Basten A, Brink R, Doherty K, Kehry MR, and Hodgkin PD: Anergic self-reactive B cells present self antigen and respond normally to CD40-dependent T-cell signals but are defective in antigen-receptor-mediated functions. Proceedings of the National Academy of Sciences of the United States of America 1994, 91(10):4392–4396. [PubMed: 7514304]
62. Goodnow CC, Crosbie J, Adelstein S, Lavoie TB, Smith-Gill SJ, Brink RA, Pritchard-Briscoe H, Wotherspoon JS, Loblay RH, Raphael K et al. : Altered immunoglobulin expression and functional silencing of self-reactive B lymphocytes in transgenic mice. Nature 1988, 334(6184):676–682. [PubMed: 3261841]
63. Yarkoni Y, Getahun A, and Cambier JC: Molecular underpinning of B-cell anergy. Immunol Rev 2010, 237(1):249–263. [PubMed: 20727040]
64. Pao LI, Famiglietti SJ, and Cambier JC: Asymmetrical phosphorylation and function of immunoreceptor tyrosine-based activation motif tyrosines in B cell antigen receptor signal transduction. J Immunol 1998, 160(7):3305–3314. [PubMed: 9531288]
65. Donahue AC, and Fruman DA: PI3K signaling controls cell fate at many points in B lymphocyte development and activation. Seminars in Cell & Developmental Biology 2004, 15(2):183–197. [PubMed: 15209378]
66. Schweighoffer E, Vanes L, Nys J, Cantrell D, McCleary S, Smithers N, and Tybulewicz VL: The BAFF receptor transduces survival signals by co-opting the B cell receptor signaling pathway. Immunity 2013, 38(3):475–488. [PubMed: 23453634]
67. Boyd AW, and Schrader JW: Mechanism of effector-cell blockade. I. Antigen-induced suppression of Ig synthesis in a hybridoma cell line, and correlation with cell-associated antigen. J Exp Med 1980, 151(6):1436–1451. [PubMed: 7381364]
68. Pinto D, Montani E, Bolli M, Garavaglia G, Sallusto F, Lanzavecchia A, and Jarrossay D: A functional BCR in human IgA and IgM plasma cells. Blood 2013, 121(20):4110–4114. [PubMed: 23550036]
69. Lee DSW, Rojas OL, and Gommerman JL: B cell depletion therapies in autoimmune disease: advances and mechanistic insights. Nature Reviews Drug Discovery 2020.

Author Manuscript Author Manuscript Author Manuscript Author Manuscript

70. Gresle MM, Butzkueven H, and Shaw G: Neurofilament Proteins as Body Fluid Biomarkers of Neurodegeneration in Multiple Sclerosis. Multiple Sclerosis International 2011, 2011:315406.

71. Parker Harp CR, Archambault AS, Sim J, Ferris ST, Mikesell RJ, Koni PA, Shimoda M, Linington C, Russell JH, and Wu GF: B cell antigen presentation is sufficient to drive neuroinflammation in an animal model of multiple sclerosis. J Immunol 2015, 194(11):5077–5084. [PubMed: 25895531]

72. Zheng B, Fuji RN, Elkins K, Yu SF, Fuh FK, Chuh J, Tan C, Hongo JA, Raab H, Kozak KR et al. : In vivo effects of targeting CD79b with antibodies and antibody-drug conjugates. Mol Cancer Ther 2009, 8(10):2937–2946. [PubMed: 19808977]

Author Manuscript Author Manuscript Author Manuscript Author Manuscript

**Key points:**

- Anti-human CD79A prevents autoimmunity in mice without significant B cell depletion
- Anti-human CD79A induces a transient form of B cell anergy
- Anti-human CD79A may silence antibody production by Plasmablasts and Plasma Cells

Author Manuscript Author Manuscript Author Manuscript Author Manuscript

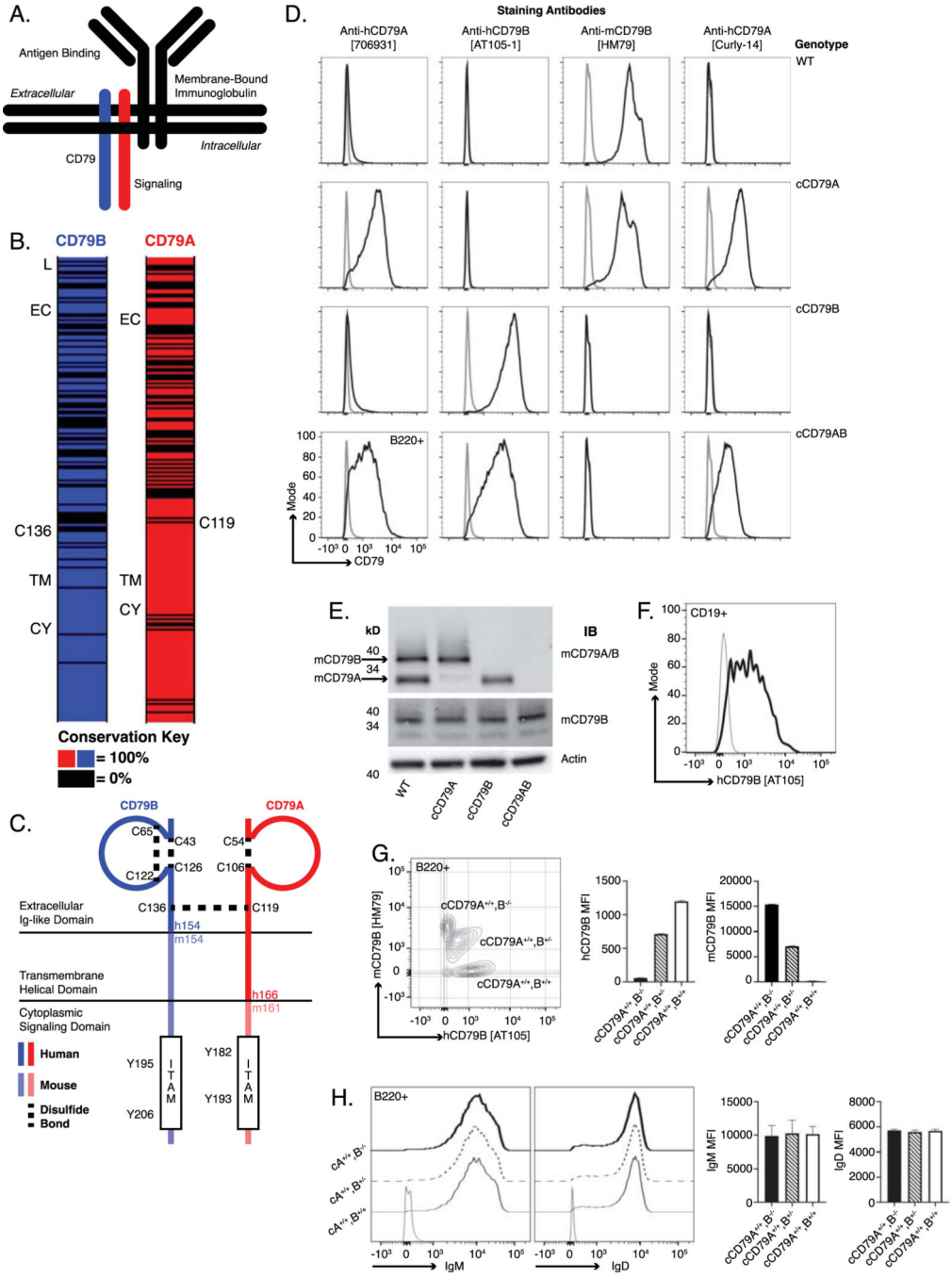


**Fig 1. Generation of chimeric human/mouse CD79 knock-in mice.**

(A.) Schematic representation of B cell antigen receptor complex. (B.) CD79 amino acid conservation between mouse and human. Black intervals represent regions of 0% amino acid conservation. Domain demarcation; L= leader, EC= extracellular, TM= transmembrane, CY= cytoplasmic. Conserved cysteines required for interchain disulfide bonding shown for each. (C.) Schematic representation of chimeric CD79. Human sequences comprise the CD79B extracellular domain and CD79A extracellular/transmembrane domains. (D.) Surface staining of splenic B cells ($B220^{+}$) from chimeric (h/m)CD79 knock-in mice

Author Manuscript Author Manuscript Author Manuscript Author Manuscript

and control C57BL/6. Gray lines show $B220^{-}$. (E.) Rabbit anti-mouse CD79 immunoblot analysis of whole cell lysates (purified splenic B cells, $CD43^{-}$) from cCD79 and WT mice. Upper membrane probed with a polyclonal rabbit antibody raised against a mouse CD79A and B extracellular domain fusion protein (Cambier lab). Middle membrane probed with a polyclonal rabbit antibody raised against the cytoplasmic domain of mouse CD79B (Cambier lab). An anti-beta actin blot was used as a protein loading control. (F.) Surface staining of B cell gated ($CD19^{+}$) human PBMCs with anti-hCD79B [AT-105]. Gray line shows $CD19^{-}$. (G.) Surface staining as a function of cCD79B allele dosage. Splenocytes from cCD79 mice of the indicated genotypes were stained with both anti-hCD79B [AT-105] and anti-mCD79B [HM79]. Gray contour shows $B220^{-}$. (H.) IgM and IgD surface expression in chimeric mice described in G. Gray line shows $B220^{-}$. n= 4 female mice per group for G and H. Error bars represent SEM. All data represents at least 3 independent experiments, representative data shown.

Author Manuscript
Author Manuscript
Author Manuscript
Author Manuscript



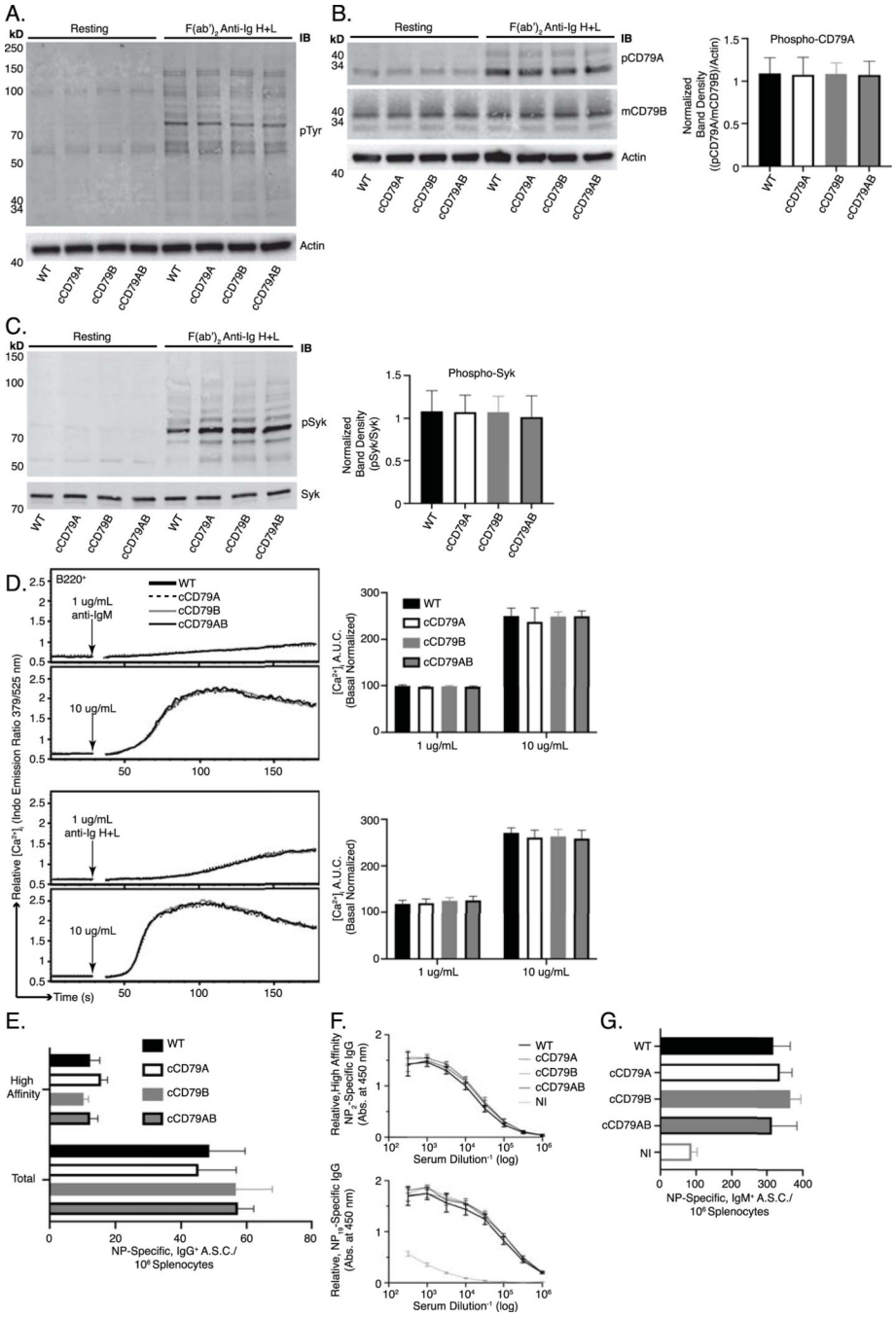


**Fig 2. BCR signaling and B cell immune responses are unaffected by expression of cCD79.**

(A.) BCR-mediated global tyrosine phosphorylation in chimeric and control B cells. 2E6 cell equivalents ($CD43^{-}$) per lane, resting or stimulated with 10 μg/mL rabbit $F(ab')_2$ anti-mouse Ig H+L for 5 min. Unstimulated cells were run in parallel (left 4 lanes) to show basal phosphorylation levels. Protein laden PVDF membranes probed with antibodies against phospho-tyrosine [4G10] and actin. (B.) BCR-mediated CD79A phosphorylation. Prepared as in A., probed with anti-phospho-CD79A (Y182) [rabbit polyclonal anti-mouse pCD79A (Y182)]. An anti-mCD79B, see Fig 1E, which recognizes the cytoplasmic tail

Author Manuscript Author Manuscript Author Manuscript Author Manuscript

of mouse CD79B, was used together with actin to normalize the relative abundance of phosphorylated mouse CD79A ((pCD79A/pCD79B)/Actin). Normalized band densities depicted to the right. (C.) BCR-mediated Syk phosphorylation. Prepared as in A., probed with anti-phospho-Syk (Y252) [polyclonal rabbit anti-pSyk (Y525/526)] and biotinylated anti-Syk [in house] followed by fluorescently-conjugated strep-avidin. Relative, normalized band densities (pSyk/Syk) depicted to the right. (D.) Representative relative intracellular free calcium before and after BCR stimulation. Splenocytes, stained with anti-B220 and loaded with Indo-1 AM, were stimulated with 1 or 10 μg/mL $F(ab')_2$ of either goat anti-mouse IgM (upper traces) or rabbit anti-mouse Ig H+L (lower), approximating IgM-only and total BCR stimulation, respectively. Post-stimulation, basal-normalized area under curve (AUC) depicted on the right. (E.) Total ($NP_{19}$-binding) and high affinity ($NP_2$-binding) $IgG^+$ ELISPOT quantification, 16 days post-immunization with NP-conjugated ovalbumin in alum. (F.) Relative serum concentrations of IgG anti-NP antibodies from mice immunized in E at 16dpi. (G.) Total ($NP_{19}$-binding) $IgM^+$ ELISPOT quantification, 7 days post-immunization with $NP_{59}$-ficoll. NI= not immunized. n= 3 male and 3 female mice per group. Error bars show SEM. All data represents at least 3 independent experiments, representative data shown.

Author Manuscript
Author Manuscript
Author Manuscript
Author Manuscript



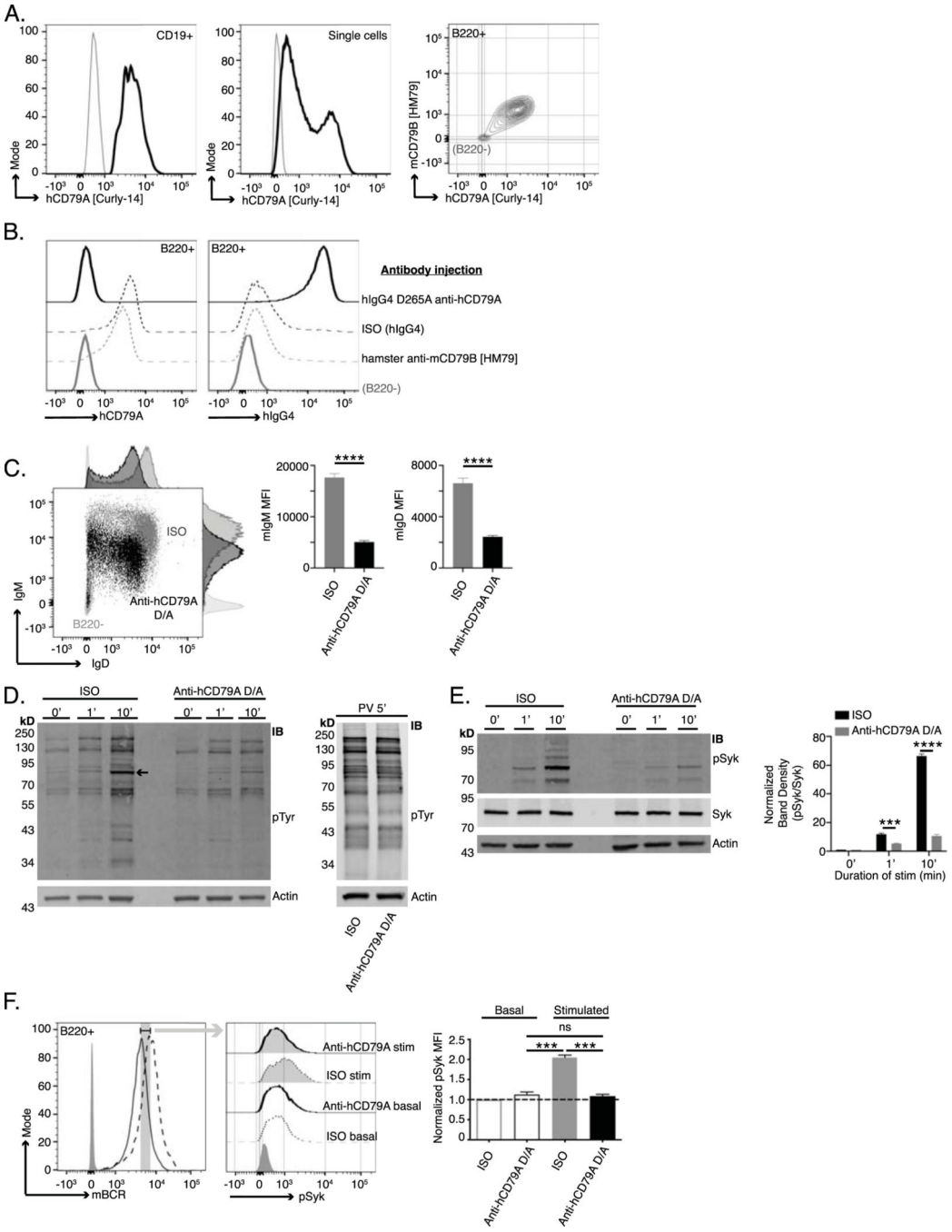


**Fig 3. Anti-human CD79A treatment induces an anergic-like phenotype in B cells.**

(A.) Surface staining of PBMCs (left) and Ramos cells (middle) with anti-hCD79A [Curly-14]. Dual staining of cCD79A$^{+/+}$B$^{-/-}$ knock-in splenocytes (right) with anti-hCD79A [Curly-14] AND anti-mCD79B [HM79]. Gray lines indicate CD19$^{-}$, ns, and B220$^{-}$ for PBMCs, Ramos, and cCD79A knock-in splenocytes, respectively. (B.) Binding of the humanized anti-hCD79A clinical candidate to cCD79A B cells. 18 hours prior to assay, cCD79A knock-in mice received 250 μg IP injections of either hIgG4 D265A anti-hCD79A (solid black), hIgG4 isotype control (dashed black), or hamster anti-mCD79B [HM79]

Author Manuscript Author Manuscript Author Manuscript Author Manuscript

(dashed gray). RBC-lysed splenocytes were stained with anti-B220 and either anti-hCD79A [Curly-14] (left) or anti-hIgG4 (right). Solid gray lines represent $B220^{-}$. (C.) Surface expression of IgM and IgD on cCD79 B cells ($B220^{+}$) 18 hours after IP injection with 250 μg of either human IgG4 D265A anti-human CD79A (black) or isotype control hIgG4 (gray). Light gray histograms show $B220^{-}$. (D.) Western blot analysis of global tyrosine phosphorylation. 18 hours prior to assay, cCD79A mice were injected IP with 250 μg of either anti-human CD79A D265A or human IgG4 isotype control. Splenic B cells were purified by CD43 exclusion and stimulated with 10 μg/mL F(ab')2 goat anti-mouse IgM for the indicated number of minutes (left) or stimulated with 1X pervanadate for 5 min (right). Whole cell lysates of 2E6 B cell ($CD43^{-}$) equivalents, both stimulated and not, were separated by SDS-PAGE and transferred to PVDF membranes. Protein-transferred membranes were blotted with antibodies against phosphorylated tyrosine [4G10] and actin. (E.) Western blot analysis of Syk phosphorylation. 18 hours prior to assay, cCD79A mice were injected IP with 250 μg of either anti-human CD79A D265A or human IgG4 isotype control. Splenic B cells were purified by CD43 exclusion and stimulated with 10 μg/mL F(ab')2 goat anti-mouse IgM for the indicated number of minutes. Whole cell lysates of 2E6 B cell ($CD43^{-}$) equivalents, both stimulated and not, were separated by SDS-PAGE and transferred to PVDF membranes. Protein-transferred membranes were blotted with antibodies against pSyk (Y525), total Syk, and actin. A densitometric summary of pSyk/Syk is shown on the right. (F.) Flow cytometric analysis of Syk phosphorylation as a function of mBCR expression. Mice were treated as in E before RBC-lysed splenocytes were stimulated as above for 5 min. Fixed cells were stained with fluorescent antibodies against B220 and mBCR. After permeabilization, cells were stained with anti-pSyk (Y525). B cells were gated on equivalent mBCR expression (left) before comparing pSyk MFIs (middle and right). Error bars show SEM. Student's t-test used to evaluate statistical significance. *, $p<0.05$; **, $p<0.01$; ***, $p<0.001$; ****, $p<0.0001$. All data represents at least 3 independent experiments, representative data shown.

Author Manuscript
Author Manuscript
Author Manuscript
Author Manuscript



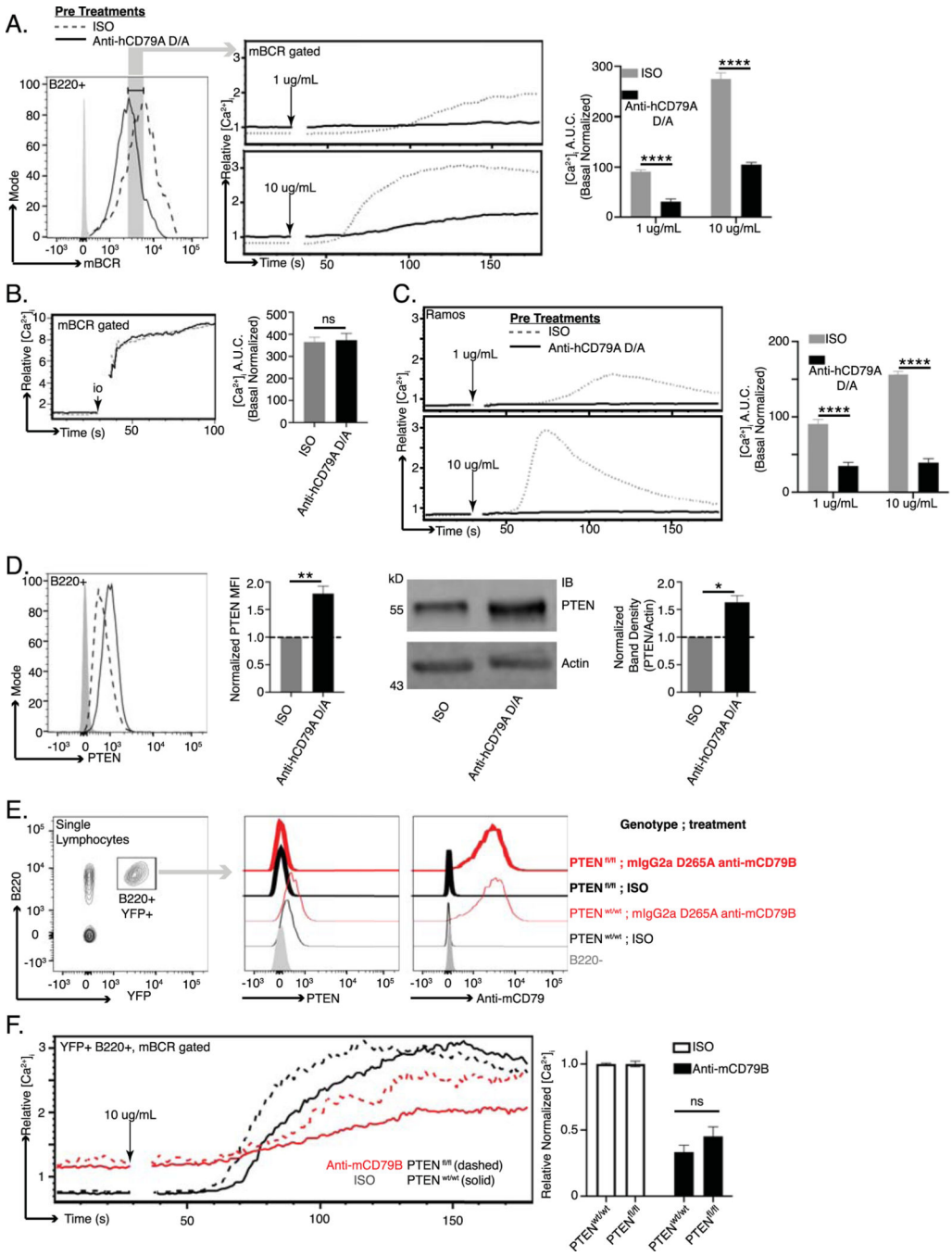


**Fig 4. Anti-human CD79A treatment induces suppression of BCR-mediated calcium mobilization.**

(A.) BCR-mediated calcium signaling in B cells from cCD79A mice receiving 250 μg IP injection of anti-human CD79A D265A or control hIgG4 24 hours prior. mBCR expression (left) was measured and gated by staining with a polyclonal goat fab anti-mouse IgG (H+L). Anti-hCD79A (solid); control hIgG4 (dashed). Cells were restimulated with 1 or 10 μg/mL rat anti-mouse IgM [B76]. Post stimulation area under the curve (AUC) was normalized to basal calcium levels (right). (B.) Cells prepared as in A. stimulated with 10 μM ionomycin. (C.) BCR-mediated calcium signaling in Ramos cells after overnight in

Author Manuscript Author Manuscript Author Manuscript Author Manuscript

vitro incubation with 25 μg/mL human IgG4 anti-hCD79A D265A (solid line) or isotype control hIgG4 (dashed line). Cells were restimulated with either 1 or 10 μg/mL goat F(ab')2 anti-human IgM Cμ5. (D.) Flow cytometric (left and MFI bar graph) and western blot (right and densitometry) analysis of PTEN expression in B cells from cCD79A animals receiving 250 μg IP injection of either anti-human CD79A D265A or control hIgG4, 24 hours prior. For flow cytometry, RBC-lysed splenocytes were fixed and permeabilized before staining with antibodies against B220 and PTEN. Gray histogram represents staining isotype control antibody. hIgG4 (dashed line), anti-hCD79A D265A (solid). For western blot, membranes were prepared as in 3D, without BCR stimulation, before being probed with antibodies against PTEN or actin. (E.) hCD20-Cre$^{TAM}$ X ROSA26-STOPflox-YFP X *PTEN*$^{flox/flox}$ or hCD20-Cre$^{TAM}$ X ROSA-26-STOPflox-YFP X *PTEN*$^{WT}$ mice were given 2 mg IP injections of tamoxifen (TAM) on d0. Day 7 post-TAM, mice were injected IP with 0.25 mg of either mouse IgG2a D265A anti-mouse CD79B or control mouse IgG2a anti-HEL. 18 hours post antibody injection, B220$^{+}$YFP$^{+}$ splenocytes were analyzed by flow for PTEN expression and antibody coating. (F.) As before, calcium was measured as a function of equal mBCR expression. n= 3 mice per group. Error bars show SEM. Student's t-test used to evaluate statistical significance. *, $p<0.05$; **, $p<0.01$; ***, $p<0.001$; ****, $p<0.0001$. All data represents at least 3 independent experiments, representative data shown.

Author Manuscript Author Manuscript Author Manuscript Author Manuscript

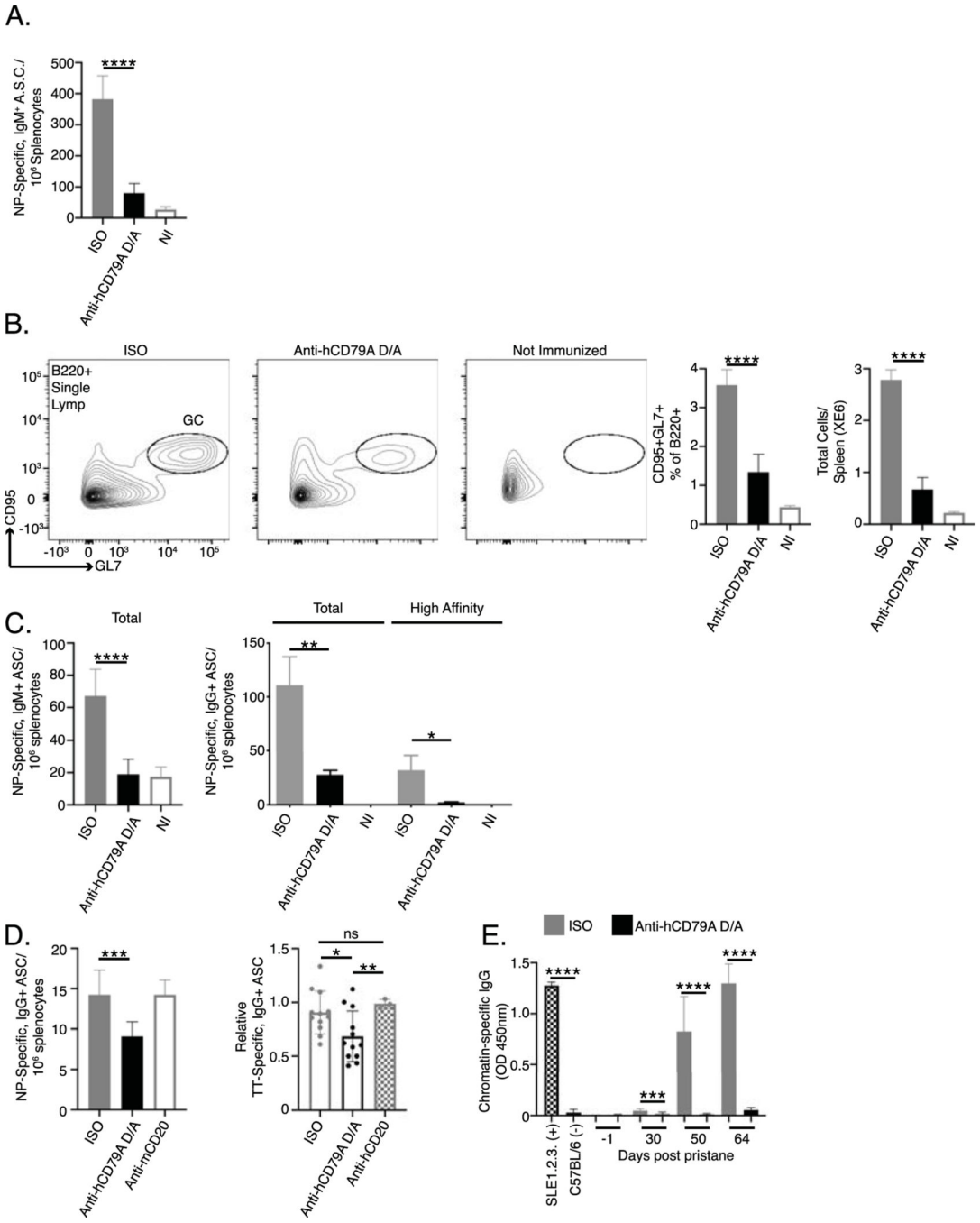


**Fig 5. Anti-human CD79A treatment inhibits B cell immune responses.**

(A.) ELISPOT analysis of NP-specific, $IgM^+$ ASC 7 days after immunization with $NP_{59}$-ficoll. 24 hours prior to immunization, cCD79A mice received 250 μg IP injections of either anti-human CD79A D265A or control hIgG4. (B.) Flow cytometric analysis of germinal center B cell induction 5 days after immunization with 0.1% SRBC in PBS. 24 hours prior to immunization, cCD79A animals received 250 μg IP injections of either anti-human CD79A D265A or control hIgG4. On day 5 post immunization, RBC-lysed splenocytes were stained with antibodies recognizing B220, CD95, and GL7. (C.) ELISPOT analysis

Author Manuscript Author Manuscript Author Manuscript Author Manuscript

of NP-specific $IgM^+$ (left) and $IgG^+$ (right) ASCs 16 days post immunization with NP-Ova in alum. 24 hours prior to immunization cCD79A mice received 250 μg IP injections of either anti-human CD79A D265A or control hIgG4. For detection of total IgM and IgG anti-NP ASC, plates are coated with $NP_{19}$-BSA. For detection of high affinity IgG anti-NP ASC, plates are coated with $NP_2$-BSA. (D.) ELISPOT analysis of NP- (left) and tetanus toxoid-specific (right) $IgG^+$ ASC following overnight incubation with anti-human CD79A D265A. NP-specific ASC were generated by immunizing cCD79A knock-in mice with NP-Ova in alum and harvesting spleens 16 days later. 10E6 RBC-lysed splenocytes were put into 1 mL cultures containing 25 μg of either anti-human CD79A D265A, anti-mouse CD20, control hIgG4, or control mIgG2a. After 18-hour incubations, cells were washed and loaded onto ELISPOT plates coated with $NP_{19}$-BSA. n= 3 wells per condition. This experiment was repeated 3 times. PBMCs were isolated from peripheral blood obtained from subjects receiving Tdap booster vaccines 7–10 days prior. 5E6 PBMCs were put into 1 mL cultures containing 25 μg of either anti-human CD79A D265A, anti-human CD20, or control hIgG4. After overnight incubation, cells were washed and loaded onto tetanus toxoid coated ELISPOT plates. n= 3 subjects who's PBMCs were incubated with anti-human CD79, n= 1 subject who's PBMCs were also incubated with anti-human CD20. Points represent individual counted wells. (E.) Effects of serial, weekly treatments with hIgG4 D265A anti-hCD79A in pristane-induced development of autoantibodies (Anti-chromatin IgG ELISAs). Pooled sera from aged/diseased SLE1.2.3 mice and wild-type C57BL/6 served as positive and negative controls, respectively. n = 20 male and 20 female cCD79A mice per treatment arm. Error bars show SEM. Student's t-test used to evaluate statistical significance. *, $p<0.05$; **, $p<0.01$; ***, $p<0.001$; ****, $p<0.0001$. All data represents at least 3 independent experiments, representative data shown.

Author Manuscript Author Manuscript Author Manuscript Author Manuscript

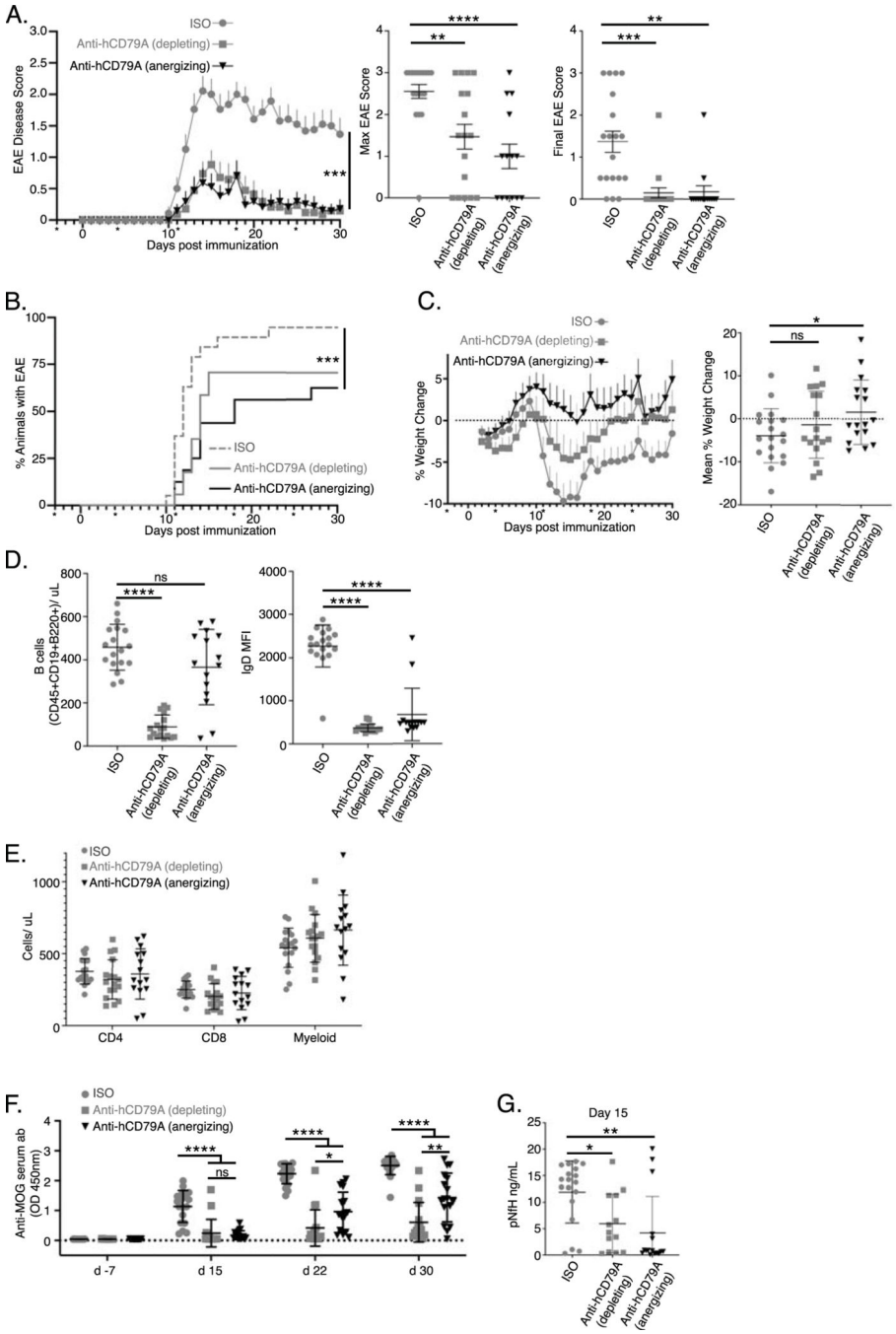


**Fig 6. Anti-human CD79 treatment prevents the development of $MOG_{1–125}$-induced experimental autoimmune encephalomyelitis.**

(A) Prophylactic treatment of EAE in mice immunized with $hMOG_{1–125}$. Anti-hCD79A mIgG2a (depleting; 20 mg/kg; n= 17 female and male mice) and aglycosyl-mIgG1 anti-hCD79A (anergizing; 20 mg/kg; n= 16 female and male) were compared with their respective anti-HEL isotype controls (mIgG2a n= 9; mIgG1 agly n= 10 female and male). Asterisks indicate day of antibody treatment. Error bars show SEM. Kruskal-Wallis with Dunn's multiple comparison test, ***, $p<0.001$. (B.) Time to EAE onset and EAE incidence based on scores only. Wilcoxon Log-Rank test, ***, $p<0.001$. (C.) Weight change of EAE

Author Manuscript Author Manuscript Author Manuscript Author Manuscript

mice over time shown as % of initial weight (left). Mean weight change shown as % of initial weight (right). (D.) Splenic B cell counts ($CD45^+CD19^+B220^+$, left) and IgD expression (right) at take down (d30) of $hMOG_{1–125}$-induced EAE. (E.) Splenocyte counts of non-B cells in EAE spleens at take down ($CD45^+CD4^+$ T cells, $CD45^+CD8^+$ T cells, $Ly6G^+Ly6C^+CD11B^+$ myeloid cells). (F.) Relative abundance (OD 450nm) of anti-MOG antibodies before EAE, during peak (d15) and chronic (d22) phases of disease, and at takedown (d30). (G.) Serum concentrations [ng/mL] of phosphorylated neurofilament heavy chain (pNfH) in EAE mice at peak of disease (d15).